

University of South Bohemia in České Budějovice, Faculty of Science

Bachelor Thesis

Characterisation of new diplomid species via electron
microscopy, starvation experiments and
immunofluorescence studies

Kristýna Cimrhanzlová
2020

Supervisor: Michael John Hammond, Ph.D.

Co-supervisor: Tashyreva Daria Ph.D.

Cimrhánzlová K., 2020: Characterisation of new diplomemid species via electron microscopy, starvation experiments and immunofluorescence studies. Bc. Thesis, in English. – 42p., Faculty of Science, University of South Bohemia, České Budějovice, Czech Republic

Annotation:

The large abundance and diversity of diplomemids in oceans has been overlooked until recently. Diplomemids are now starting to be recognised as an abundant and diverse group of the planktonic community. It is in our best interest to study these fascinating microorganisms to learn more about how they impact the ecosystems of the world's oceans. This thesis is focused primarily on morphological descriptions and determination of the life stages of four newly discovered species.

Declaration:

I hereby declare that I have worked on my bachelor's thesis independently and used only the sources listed in the bibliography.

I hereby declare that, in accordance with Article 47b of Act No. 111/1998 in the valid wording, I agree with the publication of my bachelor thesis, in full form to be kept in the Faculty of Science archive, in electronic form in publicly accessible part of the STAG database operated by the University of South Bohemia in České Budějovice accessible through its web pages.

Further, I agree to the electronic publication of the comments of my supervisor and thesis opponents and the record of the proceedings and results of the thesis defence in accordance with aforementioned Act. No. 111/1998. I also agree to the comparison of the text of my thesis with the Theses.cz thesis database operated by the National Registry of University Theses and a plagiarism detection system.

České Budějovice

.....

Kristýna Cimrhánzlová

Acknowledgment:

I would like to express my huge thanks to my supervisor Michael Hammond for helping me to improve my skills, providing expert consultations and for always being very kind and patient with me. Likewise, I would like to thank to my co-supervisor Daria Tashyreva who graciously helped me with the experiments and provided professional consultations. Also, thanks to Aleš Horák for the tremendous help with the phylogenetic analyses.

Of course, I cannot forget to thank Julius Lukeš for giving me the opportunity to work in the laboratory and allowing me to gain so much useful experience, for which I am very grateful. I am also very thankful to Jan Pyrih, Eva Kriegová and Vendula Rašková who were very helpful, especially during my first few months in the lab. Further I would like to extend thanks to all other members of the lab for helping me, being very nice to me and providing a great work culture.

Finally, I would like to thank to my partner Craig and my parents and brother, who are always supportive of me. I am grateful to have you all in my life.

Table of contents

1	Introduction.....	1
2	Aims of the Thesis	4
3	Materials and methods	5
3.1	Isolation and cultivation	5
3.2	Distinction of species and samples.....	6
3.3	DNA isolation and amplification.....	6
3.4	Phylogenetic analyses.....	8
3.5	Growth Curves.....	9
3.6	Starvation experiments	9
3.7	Fluorescence in situ hybridization (FISH) and DNA staining.....	10
3.8	Experiments with extracellular bacteria	11
3.9	Visualization of mitochondria in living cells	11
3.10	Visualization of mitochondria via immunofluorescence assay	11
3.11	Light and fluorescence microscopy	12
3.12	Scanning electron microscopy.....	12
3.13	Transmission electron microscopy	13
4	Results.....	13
4.1	Phylogenetic analyses.....	13
4.2	Light microscopy and cell cycle.....	15
4.2.1	Morphology.....	15
4.2.2	Growth curves	21
4.2.3	Starvation experiment	23
4.3	Morphology and localization of bacterial endosymbionts.....	24
4.4	Molecular phylogeny and taxonomy of endosymbionts.....	26
4.5	Experiments with extracellular bacteria	28
4.6	Fluorescence staining of mitochondria.....	28
4.7	Fine structure	30
5	Discussion.....	37
6	References.....	40

1 Introduction

Diplonemids are colourless, flagellated and heterotrophic single celled eukaryotes (David and Archibald 2016). As a result of the Tara Oceans expedition and Tara Oceans Polar Circle expedition, whose goal was to screen and collect planktonic organisms around the oceans of the world, diplonemids were distinguished from other oceanic microorganisms and have come into prominent focus for research (Lukeš *et al.* 2015). Until then, diplonemids were relatively unknown and assumed to be scarcely found in aquatic environments. Such an assumption was mainly due to their most populated habitats being the deep layers of the oceans which were comparatively less investigated (Lukeš *et al.* 2015). Diplonemids were subsequently shown to be of great abundance in the world's oceans, thought to be the most diverse group of organisms present in surface plankton communities, with abundance and diversity increasing at the depths of the oceans. Due to their recently demonstrated abundance and diversity, diplonemids are considered to play key ecological roles in planktonic communities (Flegontova *et al.* 2016).

Initially it was speculated that diplonemids exist as free-living predators, feeding on both prokaryotes and eukaryotes and that some can be even parasites or symbionts (David and Archibald 2016). More recent studies suggest that diplonemids have features commonly found in parasites or predators (Tashyreva *et al.* 2018a; Tashyreva *et al.* 2018b).

Phylogenetic and taxonomic classification of Diplonemea is currently in flux as research in this area continues to progress (Burger and Valach 2018). Diplonemids belong to the Excavata supergroup (Faktorová *et al.* 2016) which are typically characterised by the presence of a ventral feeding groove and related cytoskeletal structures (Hampl *et al.* 2009). Diplonemids are further classified to the Euglenozoa phylum (Faktorová *et al.* 2016) which can be defined by the presence of paraxial rods (Simpson 1997).

Euglenozoa contain three defined clades of Kinetoplastea, Euglenida and Diplonemea (Faktorová *et al.* 2016). The Kinetoplastea class includes many crucial human parasites which can employ bloodsucking insects as a transmission vector, e.g., *Trypanosoma brucei*, *T. cruzi*, *Leishmania donovani*, *L. major*, and *L. tropica* (Gibson 2016). The outstanding representative of the Euglenida class is the *Euglena* genus which contain mainly freshwater flagellates, including the well-known photosynthetic species *Euglena gracilis* (Faktorová *et al.* 2016; Kottuparambil *et al.* 2018). Diplonemids were recently subdivided into four lineages;

the Diplonemidae clade, Hemistasiidae clade, and deep-sea pelagic diplonemid (DSPD) clades I and II (Tashyreva *et al.* 2018b). The most well-known representative of Hemistasiidae clade is *Hemistasia phaeocysticola* which has been observed as a predator of small organisms such as Diatoms and Dinoflagellates (Yabuki and Tame 2015).

The Diplonemidae clade is further subdivided into *Diplonema*, *Rhynchopus*, *Lacrimia*, *Sulcionema* and *Flectonema* genera. Previously just two genera were recognised, according to their lifestages; diplonemids exhibiting a non-flagellated stage within their life cycle were classified into the genus *Rhynchopus*, while those with permanently protruding flagella were considered members of the genus *Diplonema* (Tashyreva *et al.* 2018b). However, as a result of recent molecular phylogenetic analysis we can now distinguish between additional genera of *Lacrimia*, *Sulcionema* and *Flectonema* (Tashyreva *et al.* 2018b).

Many other, potentially as yet unnamed genera likely also exist (Burger and Valach 2018). Taxonomic classification of key genera is shown in Figure 1.

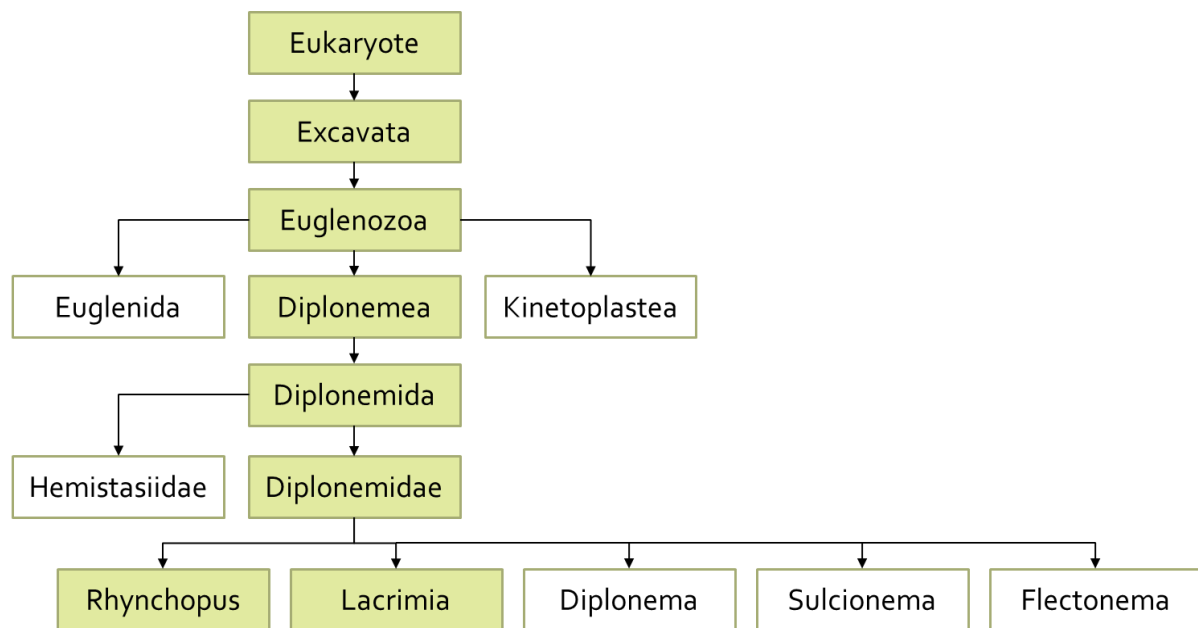


Figure 1: Taxonomic classification of key *Diplonemidae* genera (highlighted genera are discussed in this study).

Diplonemids cell sizes show high variance but are approximately 20µm in length and 5µm in width. The morphological shapes of diplonemids also differs, though most are barrel-shaped, rounded on both ends and possessing two flagella. Typically, numerous vacuoles of varied sizes are visible when observed under light microscopy. Cells are usually highly metabolic,

frequently changing shapes through contracting, extending and twisting movements (Tashyreva *et al.* 2018a).

The most well studied diplomemid species is *Diplonema papillatum*, which, along with several other diplomemids has been shown to possess an unusual mitochondrial genome. This mitochondrial DNA (mtDNA) demonstrates an abnormally large degree of fragmentation and displays a high degree of redundancy (Burger and Valach 2018). *D. papillatum* mitochondria additionally exhibit unique RNA editing systems, distinct from those seen in kinetoplasts (Burger and Valach 2018). *Diplonema* mitochondria employ substitutions of cytidine to uridine (C-to-U) and adenosine to inosine (A-to-I), and U-appendage editing. C-to-U RNA editing is relatively common in mitochondria, particularly in plants, however A-to-I substitutions are mostly restricted to the nucleus of mammals and thus the method of A-to-I editing and U-appendage RNA editing represents an unprecedented discovery (Burger and Valach 2018).

Recent research has shown that certain diplomemids harbour bacterial endosymbionts, prompted by observations of bacteria in lysed axenic cultures of *Diplonema japonicum* and *Diplonema aggregatum*. The endosymbionts in both species morphologically appear as short rods and were unable to be completely removed from the host species via antibiotic treatment (Tashyreva *et al.* 2018b). Interestingly, it was also observed that bacterial endosymbionts in diplomemids have a highly reduced genome due to adaptations to their host. The relationship between diplomemids and their endosymbionts is still mostly unexplored, but it is speculated that bacteria may manipulate the host's metabolism or play a role in defending the host against additional bacterial infections (George *et al.* 2020). Some diplomemid species also demonstrated multiple life stages; engaging in a distinct swimming stage characterised by lengthened flagella and the presence of a paraflagellar rod when placed in nutrient deficient media, and furthermore developed tubular extrusomes, representing a synapomorphic trait of Euglenozoa (Tashyreva *et al.* 2018b). Despite the aforementioned abundance of diplomemids in the world's oceans they continue to be one of the most poorly studied groups of protists (Tashyreva *et al.* 2018b).

This current investigation has focused on the characterisation of four obtained isolates that fall within the Diplonemidae clade and represent new species. Three diplomemid samples are species of *Rhynchopus* while one is a species of *Lacrimia* genus. We sought to investigate these species through phylogenetic classification, life stage analysis, ultrastructure and morphology studies as well as the verification of endosymbiont presence.

2 Aims of the Thesis

The aims of this thesis include the following:

- Classify the molecular phylogenetic positions of new diplonemid species
- Characterise morphological and ultrastructural features of these species
- Investigate the presence of endosymbionts and classify their phylogenetic positions
- Determine possible life stages of new species

3 Materials and methods

3.1 Isolation and cultivation

Clonal cultures of diplomonads were previously established from seawater samples collected in the Sea of Japan. Individual cells were selected with a microcapillary and inoculated into a seawater-based Hemi medium containing a 10 $\mu\text{l}\cdot\text{ml}^{-1}$ antibiotic cocktail (P4083, Sigma-Aldrich) (Tashyreva *et al.* 2018a). Later, cells were incubated in Hemi medium (Table 1) supplemented with horse serum and LB stock (Table 2). The concentration of sea salts in Hemi medium was 3.6%.

Table 1: Hemi medium

Reagent	Amount
Milli-Q water (Milli-Q [®] Direct 8 Water Purification System)	990ml
Sea salts (Sigma-Aldrich)	36g
Horse serum (Sigma-Aldrich)	10ml
LB stock (Table 2)	1ml

Table 2: LB stock

Reagent	Amount
Milli-Q water (Milli-Q [®] Direct 8 Water Purification System)	10ml
Tryptone (Tryptone BioChemica)	100mg
Sodium chloride (Penta)	100mg
Yeast extract bacteriological (VWR)	50mg

Cells were grown at 15 °C and transferred once a week into the new flasks to maintain healthy cultures. Usually 9 ml of new media and 1 ml of the previous culture was pipetted into the new 25cm² flask (TPP Techno Plastic Products AG). Cultures of diplomonads were frequently observed under a light microscope (Primovert microscope, Carl Zeiss Microscopy) in the interest of monitoring their life stages, motility and morphology.

3.2 Distinction of species and samples

For our study, 4 species were identified for further examination. 1 *Lacrimia* and 3 *Rhynchopus* species. 2 species (1 *Lacrimia* and 1 *Rhynchopus*) are represented here as 2 samples which, although phylogenetically identical, are differentiated by the presence/absence of bacteria. *Lacrimia* species YPF1806 have extracellular bacteria in the surrounding medium while YPF1808 does not. Similarly, *Rhynchopus* YZ270 cl. 10.3 possesses endosymbiotic bacteria while YZ270 cl.1.7 does not. These samples were compared to each other in this study. Distinction of species and samples is seen in Table 3.

Table 3: Distinction of species and samples. Scale bars are 10µm

		SPECIES			
		<i>Lacrimia</i> sp. YPF 1806 and 1808	<i>Rhynchopus</i> YZ270 cl. 1 and cl. 10	<i>Rhynchopus</i> YZ270 cl. 9	<i>Rhynchopus</i> KQ12
SAMPLES					
		1806	cl. 10.3	cl. 9	KQ12
					
		1808*	cl. 1.7**		
		*Without extracellular bacteria			
		**Without bacterial endosymbionts			

3.3 DNA isolation and amplification

DNA isolation and amplification were performed to distinguish species within the broader phylogenetic tree of Diplonemida. For isolation of DNA, 5ml of healthy culture was used for each sample. Total genomic DNA of diplonemids and endosymbionts was isolated using Exgene™ Clinic SV kit (GeneAll®) following the manufacturer’s protocol A. To distinguish eukaryotic diplonemid species, near full-length 18S ribosomal RNA (rRNA) gene was amplified via polymerase chain reaction (PCR) (Table 4), (Table 5) with universal eukaryotic primers SA (AACCTGGTTGATCCTGCCAGT)

and SB (TGATCCTCCTGCAGGTCCACCT) (Tashyreva *et al.* 2018b). Agarose gel (Table 6) electrophoresis was employed to analyse size of the amplified DNA fragments. Electric field of 70V was applied and negatively charged DNA travelled through agarose gel for 25 minutes. Results from electrophoresis were visualised on the ChemiDoc (BioRad). DNA samples were purified with MinElute PCR Purification Kit (Qiagen), to separate DNA from PCR reagents. Finally, samples were measured on NanoDrop™ 1000 Spectrophotometer (Thermo Fisher Scientific) to evaluate the concentration and purity of nucleic acids.

16S rRNA PCR represents a commonly used method for detection of bacterial species. Bacterial organisms make use of ribosome components of different sizes, with conserved genetic regions which are nonetheless distinct from eukaryotic ribosomal genes, as such, successful 16S rRNA PCR (Tables 4 and 5) of extracted DNA indicates the presence of bacterial endosymbionts in diplonemid species. Endosymbiont 16S rRNA gene was amplified with bacteria-specific 16S forward (GCTTAACACATGCAAG) and reverse (CATTGTAGCACGTGT) primers, providing amplicons which were sequenced. The procedure was the same as that described for 18S PCR, except that the annealing and extension temperatures were altered to account for the difference in GC content of the primers (Tables 4 and 5) (Tashyreva *et al.* 2018b).

Table 4: Solution for PCR

Reagent	Amount
OneTaq® 2X Master Mix with Standard Buffer (New England Biolabs)	12.5µl
Forward primer	0.5µl
Reverse primer	0.5µl
10-20ng of DNA sample	2.0µl
Milli-Q water (Milli-Q® Direct 8 Water Purification System)	9.5µl

Table 5: Temperatures for PCR

Cycle	18S rRNA PCR		16S rRNA PCR		
	Temperature	Time	Temperature	Time	
Initial denaturation	94°C	3min	94°C	3min	
Denaturation	94°C	30sec	94°C	30sec	35x times
Annealing	58°C	30sec	55°C	30sec	
Extension	68°C	2min 20sec	68°C	1min 20sec	
Final extension	68°C	5min	68°C	5min	

Table 6: 1% Agarose Gel

Reagent	Amount
Agarose	1g
1x TAE	100ml
Ethidium Bromide	2µl

3.4 Phylogenetic analyses

Taxonomy identification is based on phylogenetic analysis. 18S rRNA sequences of novel diplomonid strains were assembled with Geneious software (Kearse *et al.* 2012), and added to the dataset containing diplomonid species covering currently recognized diplomonid diversity from families Diplonemidae, Hemistasiidae, Eupelagonemidae as well species from sister clade kinetoplastids. The dataset was aligned with newly sequenced cultures using the genafpair algorithm as implemented in Mafft v7. 450 (Katoh and Standley 2013). Ambiguous regions were removed by Gblocks Server (Talavera and Castresana 2007) using the least stringent settings (smaller final blocks, gap positions within the final blocks and less strict flanking positions). The phylogeny was reconstructed using RAxML 8.2.11 (Stamatakis 2014) under the gamma corrected GTR model with the number of bootstrap replicates set to 300. The same methods were used for 16S rRNA sequences except that a different dataset with bacteria from Holosporaceae, Rhodospirillales, Rhodobacterales, Sphingomonadales, Rhizobiales and Rickettsiales orders were used. These clades were chosen based on previously published results (Tashyreva *et al.* 2018, Prokopchuk *et al.* 2019).

3.5 Growth Curves

Growth curves are used to determine the maximum concentration which cell cultures can grow to, as well as information on their rate of growth. Using alternate species YPF1806 and clone 1.7, we also sought to learn if endosymbiont or extracellular bacteria had an impact on growth rates or maximum cell concentrations. To measure the growth rate of diplonemid species, 3 flasks with 25cm² volume (TPP Techno Plastic Products AG) and 3 well plates with 12 wells (TPP Techno Plastic Products AG) were used for each cell line. Well plates were sealed with parafilm (PARAFILM® M, Bemis Company, Inc.) after each count to protect against contamination and drying out. Cell lines started with a cell concentration of 5.10⁴ cells/ml. 10ml of prepared concentration were pipetted in each flasks and 4 ml for each well. Counting was performed 3 times a week for 21 days. Flasks were gently agitated before counting to dislodge cells from the flask bottom and ensure a homogenous distribution. 10µl of culture was used for counting 4 squares. While taking samples from well plates the cell scraper S (TPP Techno Plastic Products AG) were used for the same purpose. Each well was used just once. 8 squares were counted using cell counting Neubauer chambers for each sample. While counting samples YPF1808 and YPF1806, an agarose solution made from 100mg of agarose powder (type IX, Ultra-low Gelling Temperature, Sigma-Aldrich) and 10ml of seawater was used in ratio 1:1 with sampled *Lacrimia* to slow down their movement for easier counting. When using ratio 1:1 sum of counted cells were multiplied by 2. Because 3 flasks and 3 well plates were used, their average value of cell/ml was made.

$$cells/ml = \frac{sum\ of\ counted\ cells\ per\ 8\ squares}{8} \times 10000$$

Equation 1: Calculation of cells/ml for diplonemids species

3.6 Starvation experiments

The aim of starvation experiments was to observe if additional life stages would develop in our species, as has been seen in other diplonemids (Tashyreva *et al.* 2018b). For starvation experiments, 10ml of well grown culture was pelleted by centrifugation of 2000xg for 15 minutes at 4°C (Eppendorf® 5810 Multipurpose Centrifuge). Afterwards the pellet was re-suspended in 15ml of seawater, (Table 7) followed by another centrifugation step and final

resuspension in 15ml of new seawater, which was then placed in a new flask. Changes were observed under the microscope hourly for the first 6 hours and every 24 hours beyond that.

Table 7: Artificial sea water reagents

Reagent	Amount
Milli-Q water (Milli-Q® Direct 8 Water Purification System)	1000ml
Sea salts (Sigma-Aldrich)	36g

3.7 Fluorescence in situ hybridization (FISH) and DNA staining

FISH was employed to visualise possible bacterial endosymbionts within our samples. Cl. 1.7, cl. 10.3 and KQ12 were pelleted by centrifugations 2000xg for 5 minutes (MiniSpin® plus, eppendorf) and fixed with 4% seawater-based paraformaldehyde (BioChemica) for 30 min, after which, cells were centrifugated again and re-suspended in distilled water. Cell suspensions were applied on poly-L-lysine-coated glass slides and air-dried. Adhered cells were de-hydrated with 50, 80 and 96% ethanol solutions for 3 min each. The slides were treated with a hybridization buffer (Table 8) containing 35% (v/v) formamide and 5 ng·µl⁻¹ EUB338 probe (5'-GCTGCCTCCCGTAGGAGT-3') labelled with 5'-Cy3 fluorescent dye. The samples were incubated in humidity chambers at 46°C for 90 min, followed by incubation in washing buffer (Table 9) on a shaker at 48°C for 30 min. Finally, the slides were rinsed with distilled water and air-dried. Samples were directly mounted in ProLong Gold antifade reagent (Life Technol.) containing 4',6-diamidino-2-phenylindole (DAPI) (Tashyreva *et al.* 2018b).

Table 8: Hybridization buffer – 50ml

Reagent	Amount
5M NaCl	9ml
1M Tris/HCl	1ml
Formamide	17.5ml
10% SDS	50µl
Distilled water	22.45ml

Table 9: Washing buffer – 500ml

Reagent	Amount
5M NaCl	7ml
1M Tris/HCl	10ml
10% SDS	500µl
distilled water	482.5ml

3.8 Experiments with extracellular bacteria

10ml of culture YPF1806 were filtered through a 1µm sterile filter to separate bacteria from diplomonads. Bacteria were cultivated at 15°C. In order to investigate whether *Lacrimia* are able to ingest bacteria, culture YPF1808 and bacteria contamination were co-cultured (1:1) for 2 hours. Prior to co-cultivation bacteria were centrifugated 2000xg for 5 minutes, re-suspended in 200µl of seawater and stained with 2µl of 100µM SYTO 24 for 15 minutes. Subsequently redundant stain was washed out with 500µl of seawater few times and stained bacteria were co cultured with YPF1808 pellet.

3.9 Visualization of mitochondria in living cells

1,5ml of live cell samples were treated for 30min with SYTO 24 (Thermo Fisher Scientific) stain which binds to nucleic acids and can also stain living cells. As a result, it is possible to view the mitochondria (Table 10). Samples were pelleted by centrifugation of 2000xg for 5 minutes and washed twice with 1,5ml of seawater. Finally, 100µl of media were added to the pellet and re-suspended.

Table 10: Concentrations of SYTO 24

Colour	Initial concentration	Final concentration	Amount used on 1,5ml diplomonads
SYTO 24	100µM	0.2µM	3µl

3.10 Visualization of mitochondria via immunofluorescence assay

Immunofluorescence assay (IFA) was performed using antibodies generated in rabbit against ATPase. This antibody was employed due to ATPase being an enzyme which is highly abundant in mitochondria. Immunofluorescence assays were performed on cl. 10 and cl. 9. Cells were spun down at 2000xg for 5 minutes and fixed with 4% paraformaldehyde (BioChemica) in seawater for 30 minutes followed by washing with distilled water.

Afterwards, cells were placed on slides and permeabilised with 100% ice-cold methanol for 20 minutes. Subsequently, cells were washed with PBS (Phosphate-buffered saline), blocked for 45 minutes in 5% milk in PBS-T (0.005% Tween) while being kept in a humidity chamber and washed with PBS again. 250µl of primary antibody diluted to a 1:500 ratio (1µl antibody in 500µl of 5% milk/ PBS-T) was pipetted onto the slide, covered with parafilm and incubated at 4°C in a humidity chamber overnight. Slides were washed 3x with PBS for 5 minutes. 250µl of secondary goat anti-rabbit antibody (Alexa Fluor 488, Thermo Fisher scientific) at a 1:500 ratio (1µl antibody in 500µl of 5% milk/ PBS-T) were pipetted to each slide, which were then covered with parafilm (PARAFILM® M, Bemis Company, Inc.) and incubated for 1 hour in the dark. Slides were then washed 3x with PBS and mounted in ProLong Gold antifade reagent (Life Technol.) containing DAPI. Slides were stored at 4°C in the dark until viewing.

3.11 Light and fluorescence microscopy

Light microscopy was performed using Olympus BX53 equipped with differential interference contrast (DIC). All slides labelled with fluorescent dyes were observed with the AxioPlan 2 fluorescence microscope (Carl Zeiss Microscopy GmbH, Jena, Germany). For live imaging, a small amount of sample was placed between a slide and a cover glass. Images and videos were captured with a DP73 microscope digital camera (Olympus DP73 Universal Camera) at 1600×1200-pixel resolution using CellSens software v. 1.11 (Olympus). The images were processed using Irfan view v. 4.54 and Fiji v. 1.52 software. Fiji v. 1.52 software was also used for measurements of cells (Tashyreva *et al.* 2018b).

3.12 Scanning electron microscopy

Scanning electron microscopy enables detection of small morphological details present on the cell surface. For scanning electron microscopy (SEM), cl. 10.3, cl. 1.7, cl. 9, YPF1808 and KQ12 pellets were placed in two fixative solution for comparison. One fixative solution was made from 1% osmium tetroxide in 3.6% of seawater (250µl of osmium tetroxide, 250µl of distilled water and 500µl of 7.2% seawater). Second fixative solution was made from 1,5ml of 4% paraformaldehyde (BioChemica) with addition of 6µl of glutaraldehyde (Wanted concentration of glutaraldehyde was 0.4%). After fixations samples with osmium tetroxide were washed 3x times with distilled water while samples with paraformaldehyde were washed once. Additionally, pellets were re-suspended in 100µl of distilled water and this suspension was released as micro drops onto a thin aluminium container floating on a liquid nitrogen. Samples underwent sublimation at - 187°C for 1 hour, - 93°C for 5-6 hours, after which

temperature was slowly transitioned back to room temperature (Small and Marszalek 1969). The samples were mounted on a SEM specimen stub, coated with gold in Sputter Coater Polaron chamber, and observed with a JEOL JSM-7401F (Jeol Europe, Prague, Czech Republic) microscope at an accelerating voltage of 4 kV (Tashyreva *et al.* 2018b).

3.13 Transmission electron microscopy

Transmission electron microscopy (TEM) enables visualisation of intracellular details such as organelle distribution in cells. Samples for TEM were processed by high pressure freezing technique according to the previous article (Yurchenko *et al.* 2014) Observations were performed on JEOL JEM – 1010 1 (Jeol Europe) transmission electron microscope at accelerating voltage of 80 kV.

4 Results

4.1 Phylogenetic analyses

Maximum-likelihood analysis of an 18S rRNA gene data set with extensive sampling of members from the *Diplonemidae* clade confirmed the placement of the newly described species within the *Rhynchopus* and *Lacrimia* genera (Figure 2). Cl. 10.3, cl. 1.7, cl. 9 and KQ12 cluster to the *Rhynchopus* genus while YPF1808 and YPF1806 sorts to the *Lacrimia* genus.



Figure 2: Maximum-likelihood (ML) phylogeny of new diplonemid species (bold font) based on a 18S rRNA data set inferred in RAxML 8.2.11 under the gamma-corrected GTR model. Bold lines represent absolute support (100 BS/1.0 PP).

4.2 Light microscopy and cell cycle

4.2.1 Morphology

Healthy trophic cells of cl. 10.3 display elongated elliptical shape with rounded ends. Some appear to be narrowed on one end only (Figure 3D). The cells measure 12.5 to 19.8 (mean \pm SD [standard deviation of mean], 15.7 ± 1.6 [$n = 50$]) μm in length and 3.3 to 7.5 (4.9 ± 0.7) μm in width. While in trophic stage flagella are not visible. In fresh cultures, cells mostly glide on the bottom of the culture flasks. Cells often dramatically change their shape. They show extension, flexion, shrinking and twisting. Numerous vacuoles are spread throughout the cytoplasm. The papilla (Figure 3A, C, E) and ingestion apparatus (Figure 3B) are readily visible under transmitted light. Cells in old cultures slowly change their shape from elongated to spherical and become smaller in size. These same traits are seen in cl. 1.7 (Figure 4), but interestingly the cells measure 12.7 to 21.5 (17 ± 2.4 ; $n = 50$) μm in length and 2.5 to 7 (4.7 ± 1) μm in width, showing a slight deviation in cell length ($1.3\mu\text{m}$) potentially as a result of endosymbiont absence.

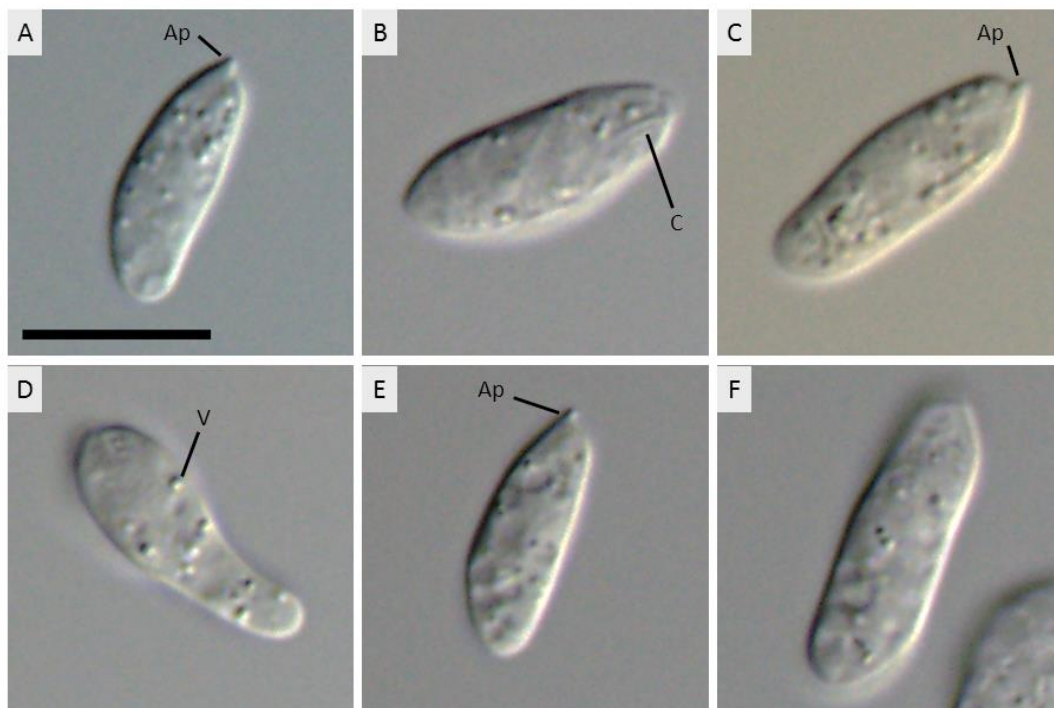


Figure 3: Differential interference contrast images of living cl. 10.3. Varied sizes of trophic cells with an elongated shape (A, B, C, E, F) and club-like shape (D); note the apical papilla (Ap), cytopharynx (C) and vacuole (V). Scale bar is $10\mu\text{m}$.

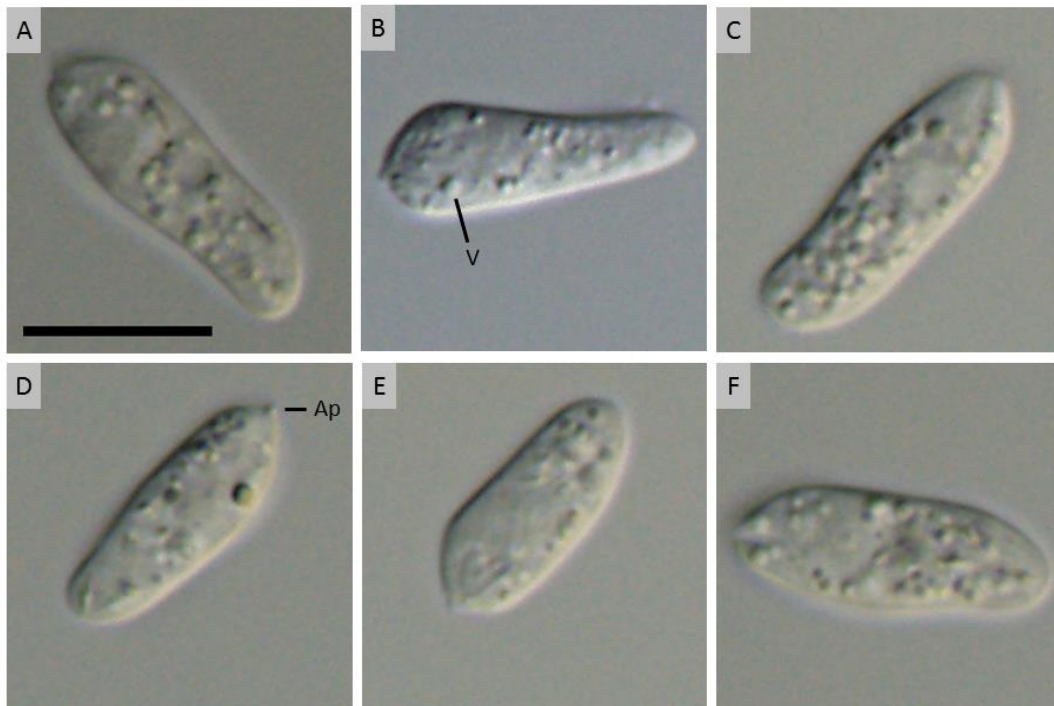


Figure 4: Differential interference contrast images of living cl. 1.7. Varied sizes of trophic cells with an elongated shape (A, C, D, E, F) and club-like shape (B); note the apical papilla (Ap) and vacuole (V). Scale bar is 10 μ m.

Cl. 9 share similar shape and features with cl. 10.3 and 1.7 with length of 10.6 to 20.7 (13.9 ± 1.9 ; $n = 50$) μ m and 3.3 to 5.9 (4.7 ± 0.6) μ m in width. However, when stressed or in older cultures cl. 9 become mainly spherical in shape (Figure 5).

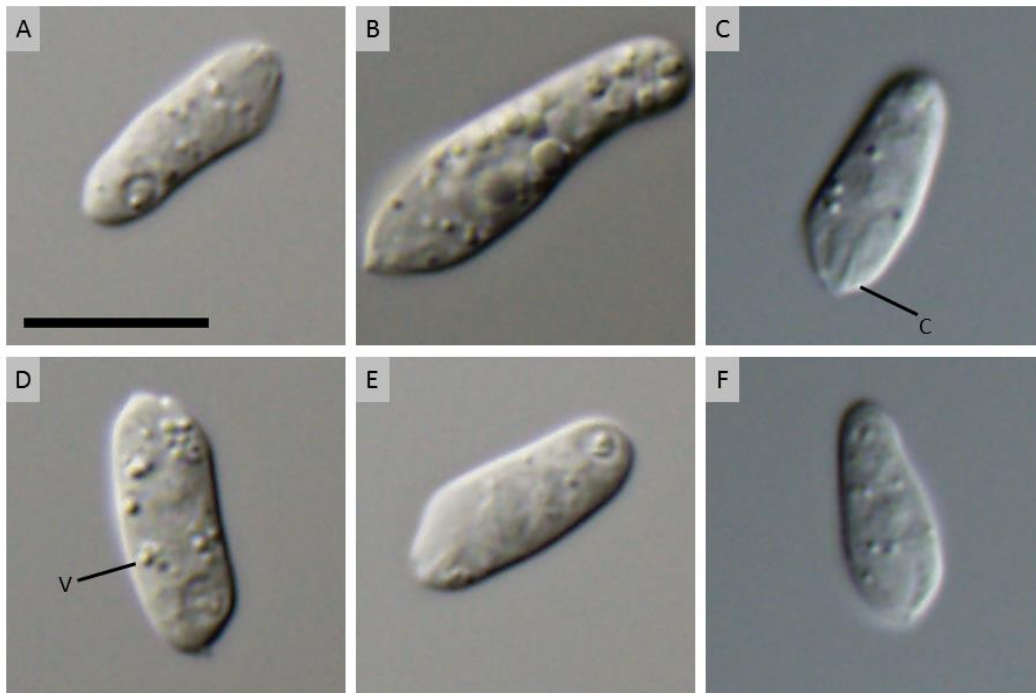


Figure 5: Differential interference contrast images of living cl. 9. Varied sizes of trophic cells with an elongated shape (A, C, D, E, F) and club-like shape (B), note the cytopharynx (C) and vacuole (V). Scale bar is 10 μ m.

KQ12 display mainly elliptical shape with one narrowed end. Many also display the shape of a cudgel or tennis racket with one end larger than the other (Figure 6). Cells measure 13.2 to 23 (17.4 ± 1.9 ; $n = 50$) μ m in length and 3.5 to 6.3 (4.7 ± 0.7) μ m in width. In the trophic stage, cells do not present flagella. In fresh cultures, cells mostly glide on the bottom of the culture flasks. Cells regularly change their shape. They also show extension, flexion, shrinking and twisting and likewise numerous vacuoles of varied sizes are spread throughout the cytoplasm.

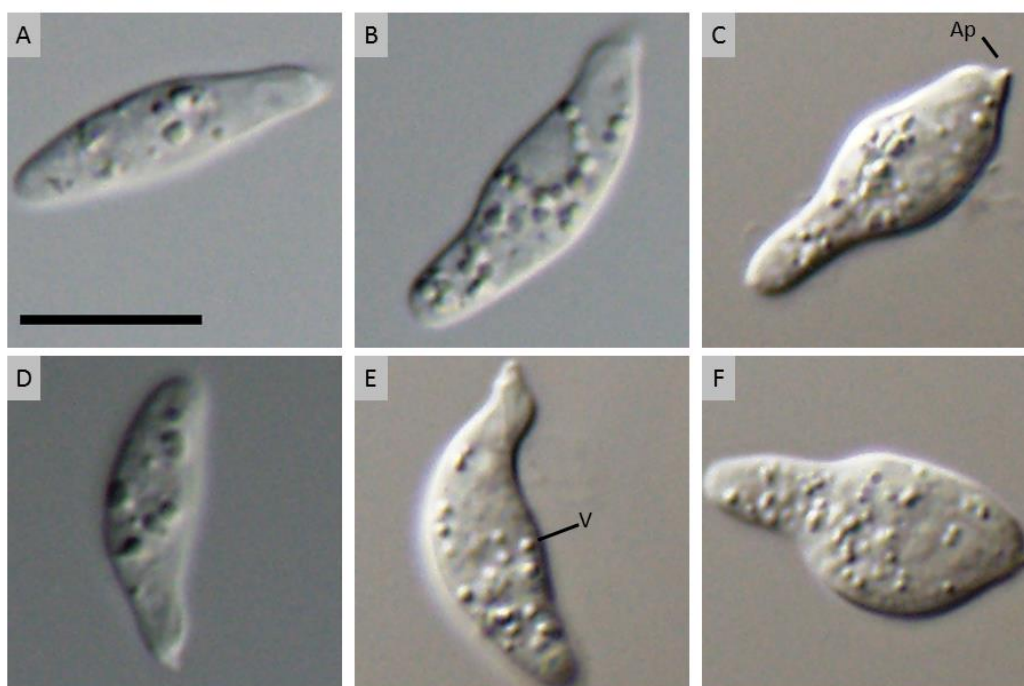


Figure 6: Differential interference contrast images of living KQ12. Varied sizes of trophic cells with an elongated shape which has one noticeable narrowed end (A, B, D, E), cudgel-like shape (C) and tennis racket-like shape (F); note the apical papilla (Ap) and vacuole (V). Scale bar is 10 μ m.

YPF1808 in well-growing cultures show two behaviours – slow swimming and fast swimming behaviour (Figure 7). When in slow swimming behaviour, cells are shaped like a teardrop. Cells normally present two flagella. The cells measure 13.3 to 22.1 (17.1 ± 2.2 ; $n = 50$) μ m in length, 5.6 to 11.4 (8.7 ± 1.4) μ m in width and flagella length measure 17.8 to 29.3 (22 ± 4.2 ; $n = 11$) μ m. Cells are generally very fluid in their behaviour but usually in fresh cultures slow swimming behaviour outnumber those with fast swimming behaviour while in older cultures fast swimming behaviour outnumbers slow swimming behaviour. Many vacuoles with different sizes are present. It is common to see one large vacuole in posterior part of the cell and many small vacuoles in anterior part of the cell. These same traits are present in YPF1806 (Figure 8). The cells of YPF1806 measure 12.4 to 24.3 (17.4 ± 2.5 ; $n = 50$) μ m in length, 4.4 to 13.4 (7.5 ± 2.2) μ m in width and flagella length measure 12 to 34.9 (21.2 ± 5.8 ; $n = 11$) μ m. Summary of key features are shown in Table 11.

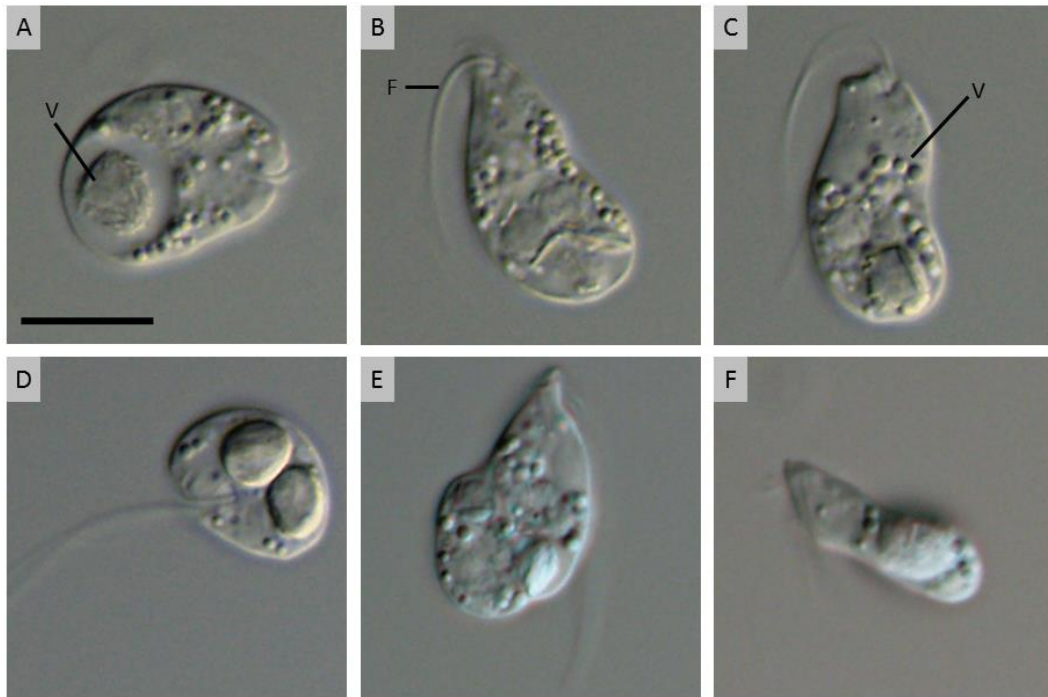


Figure 7: Differential interference contrast images of living YPF1808. Slow swimming cells (A, B, C, D, E) and a fast swimming cell (F). Slow swimming cells with drop-like shape (B, C, E) and egg-like shape (A, D) due to metabolic movements. A fast swimming cell with elongated slimmer shape (F); note the large posterior vacuole (V), flagella (F) and small vacuole (V). Scale bar is 10 μ m.

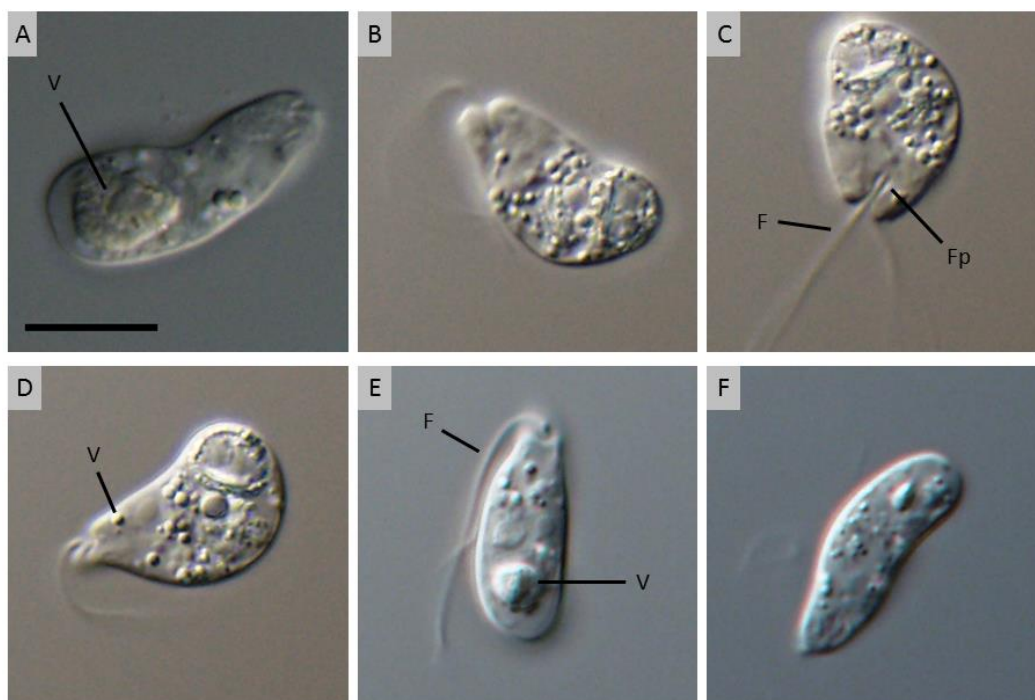


Figure 8: Differential interference contrast images of living YPF1806. Varied sizes of slow swimming cells (A, B, C, D) and fast swimming cells (E, F). Slow swimming cells with elongated drop-like shape (A, B, D) and egg-like shape (C) due to metabolic movements. Swimming cell with prolonged slim shape (E, F); note the large posterior vacuole (V), small vacuole (V) and flagella (F). Scale bar is 10 μ m.

Table 11: Summary of key features in new species

Sample	cl. 10.3	cl. 1.7	cl. 9	KQ12	YPF1808	YPF1806
Usual Cell shape	Elongated, elliptical	Elongated, elliptical	Elongated, elliptical	Elongated, elliptical	Teardrop	Teardrop
Cell size in μm	12.5 - 19.8 x 3.3 - 7.5	12.7 - 21.5 x 2.5 - 7	10.6 - 20.7 x 3.3 - 5.9	13.2 - 23 x 3.5 - 6.3	13.3 - 22.1 x 5.6 - 11.4	12.4 - 24.3 x 4.4 - 13.4
Flagella	Buried in flagellar pocket	Buried in flagellar pocket	Buried in flagellar pocket	Buried in flagellar pocket	Visible 17.8 - 29.3 μ m	Visible 12 - 34.9 μ m
Usual movement	Gliding, metabolic	Gliding, metabolic	Gliding, metabolic	Gliding, metabolic	Swimming, metabolic	Swimming, metabolic

4.2.2 Growth curves

Results of growth curves showed that some species reach higher concentrations when grown in flasks rather than in well plates (Figure 9 and 10). This is seen mainly in cl. 1.7 which in flasks reached a top density of 9.8×10^5 cell/ml (mean \pm SD, $9.8 \times 10^5 \pm 62161.58$ [$n = 3$]) meanwhile in well plates, a concentration of $8.3 \times 10^5 \pm 138204.6$ cell/ml [$n = 3$] was achieved. The same observation is seen in KQ12, when in flasks this species reached concentrations of $3.7 \times 10^5 \pm 34663.56$ cell/ml [$n = 3$] and in well plates $3 \times 10^5 \pm 43053.99$ cell/ml [$n = 3$]. Higher cell concentrations in flasks might be caused by larger surface area which they provide, enabling more space for these primarily surface-adherent species. However, cl. 9 had slightly higher concentration in well plates ($1.6 \times 10^5 \pm 7107.801$ cell/ml [$n = 3$]), than in flasks ($1.4 \times 10^5 \pm 16072.75$ cell/ml [$n = 3$]). Additionally, YPF1808 showed slightly higher concentration in well plates ($4 \times 10^5 \pm 37610.95$ cell/ml [$n = 3$]) rather than in flasks ($3.4 \times 10^5 \pm 52380.82$ cell/ml [$n = 3$]).

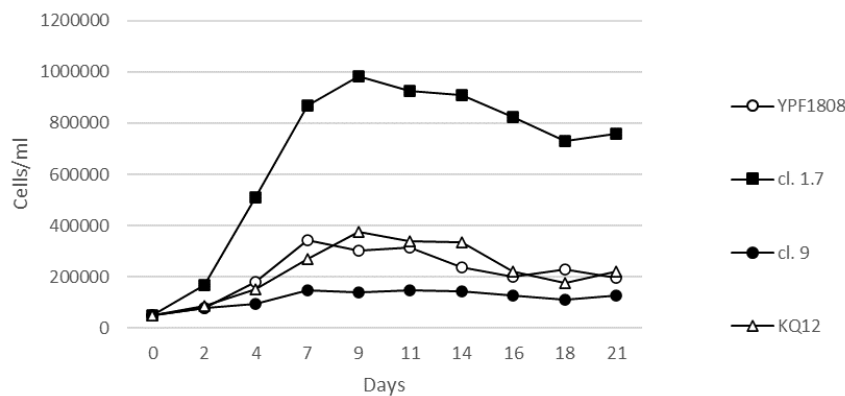


Figure 9: Growth curve of species in 10ml flask.

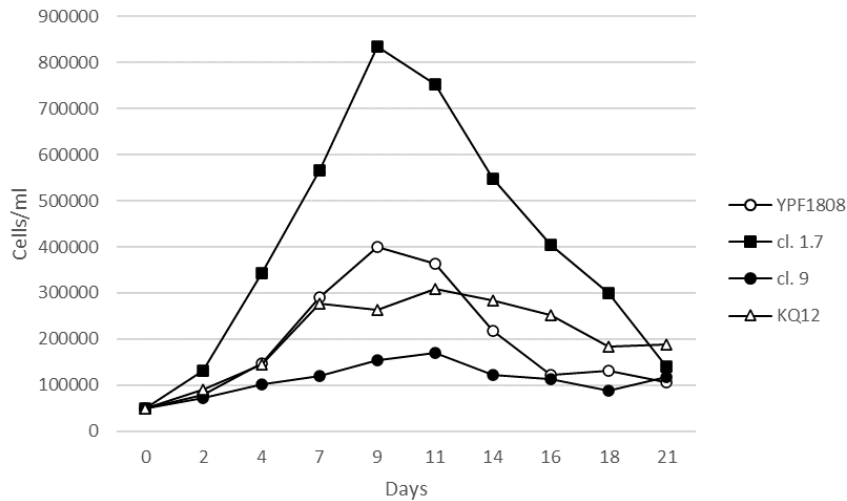


Figure 10: Growth curve of species in well plate (4ml per well).

While studying impact of endosymbionts on growth curves, no noticeable effect was observed between 1.7 and 10.3 (Figure 11). Growth curves displayed similar values throughout the observed time. Cl. 1.7 reached a top concentration of $9.8 \times 10^5 \pm 62161.58$ cell/ml [n = 3] and cl. 10.3 even $1 \times 10^6 \pm 72157.96$ cell/ml [n = 3] (Figure 11).

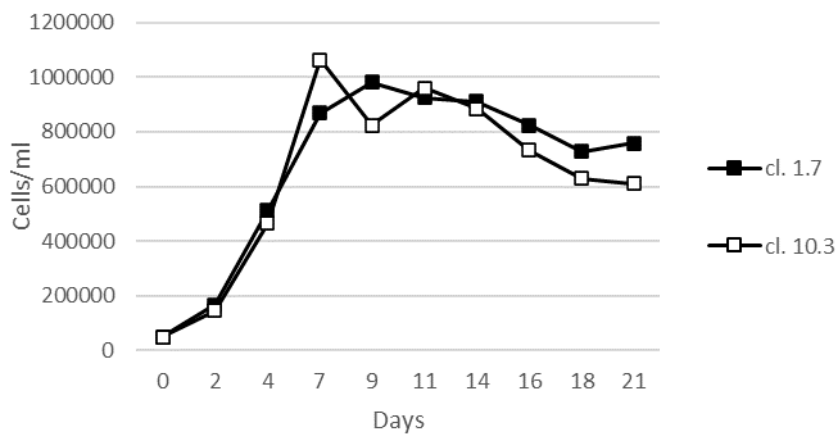


Figure 11: Growth curve of cl. 1.7 and cl. 10.3 in flasks.

Similarly, the impact of extracellular bacteria on growth curves were not seen and growth curves had again similar values for the whole experiment (Figure 12). YPF1808 reached concentration $3.4 \times 10^5 \pm 52380.82$ cell/ml [n = 3] and YPF1806 reached concentration $3.6 \times 10^5 \pm 11814.54$ cell/ml [n = 3].

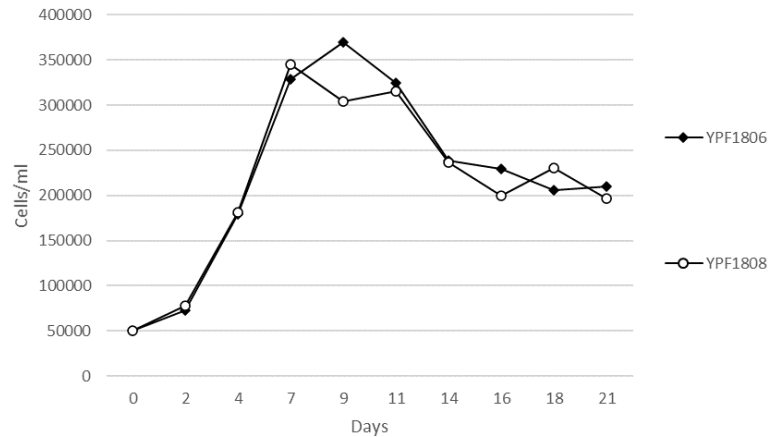


Figure 12: Growth curve of YPF1806 and YPF1808 in flasks.

Conclusively, cl. 10.3 and 1.7 displayed the highest concentrations. YPF1808, YPF1806 and KQ12 displayed very similar values in growth curves while cl. 9 showed the lowest concentration.

4.2.3 Starvation experiment

Observations from starvation experiments showed us no changes in life stages for cl. 9 species. This species was, when suspended in nutrient deprived conditions, observed changing shape from a long to spherical shape within hours, and on the fifth day, cells started to die. However, cl. 10.3, cl. 1.7 and KQ12 showed cells displaying swimming stages when placed in sea salt solution without nutrition. At first there were no differences between life stages in cl. 10.3 and cl. 1.7. Both started to detach from the bottom of the flask in 24 hours and every day after that it was possible to observe more cells that had detached. 48 hours from the start of the experiment, it was possible to detect a few swimming cells in both cultures. Swimming cells are typically slimmer than trophic cells and display two flagella. Beyond day two, it was not possible to observe any swimming cells, except on the sixth day from the start of the experiment when it was possible to observe few swimming cells in cl. 10.3 cultures. Cells of both cultures gradually shortened in size and by the eleventh day begun to die. Cells of KQ12 started changing shape from long to spherical cells after five hours. Most of the cells were spherical in one day. 24 hours from the start of the experiment, it was possible to witness swimming cells. A minority of cells were swimming through the whole experiment even when they started to die, which was on approximately the fifth day. There were no differences between behaviours in YPF1808 and YPF1806. Both samples are very fluid in their behaviours but started to swim more actively after one hour in artificial sea water and both started to make

aggregates within three hours. In 24 hours, a minority of cells were swimming while most of them were forming aggregates. While aggregation was occurring, cells were slowly grouping together into small clusters and did not show much movement or activity. In 48 hours, it was possible to see many cells swimming fast and in four days the majority of cells were displaying fast swimming behaviour. On the sixth day post-starvation it was observed that some cells started to die while others were still actively swimming. Observations of swimming stage in artificial sea water are shown in Table 12.

Table 12: Observation of swimming cells in nutrition free medium

Sample	cl. 9	cl. 10.3	cl. 1.7	KQ12
Swimming stage identified	X	✓	✓	✓

4.3 Morphology and localization of bacterial endosymbionts

Endosymbiotic bacteria were observed in cl. 10.3 (Figure 13) and KQ12 (Figure 14). Cl. 1.7 (Figure 13) were used for comparison against cl. 10.3, since no endosymbionts are present in cl. 1.7. Hybridization with the EUB338 probe, which effectively targets most bacterial groups as the probe is complementary to a conserved 16S rRNA region, exposed several bacterial cells distributed throughout the host cytoplasm. The signal was never detected extracellularly. Bacteria appear to be rod-shaped and the number of bacteria per cell was not stable (Figure 13 and 14).

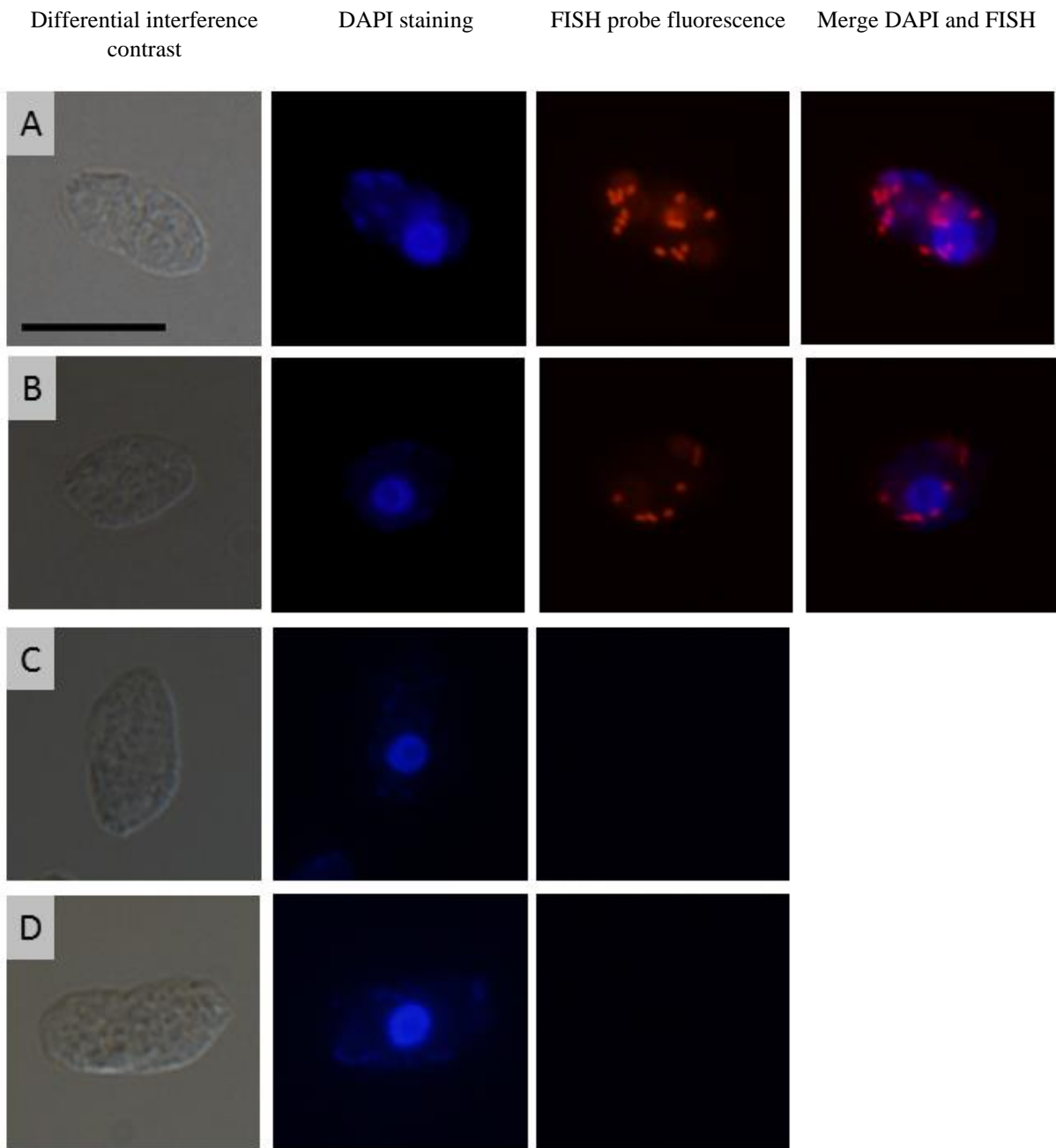


Figure 13: Comparison of differential interference contrast and fluorescence micrographs of cl. 10.3 (A, B) and 1.7 (C, D). Shown from left to right are a differential interference contrast image, DAPI staining, FISH probe fluorescence, and overlaid DAPI and FISH images. Scale bar is 10 μ m.

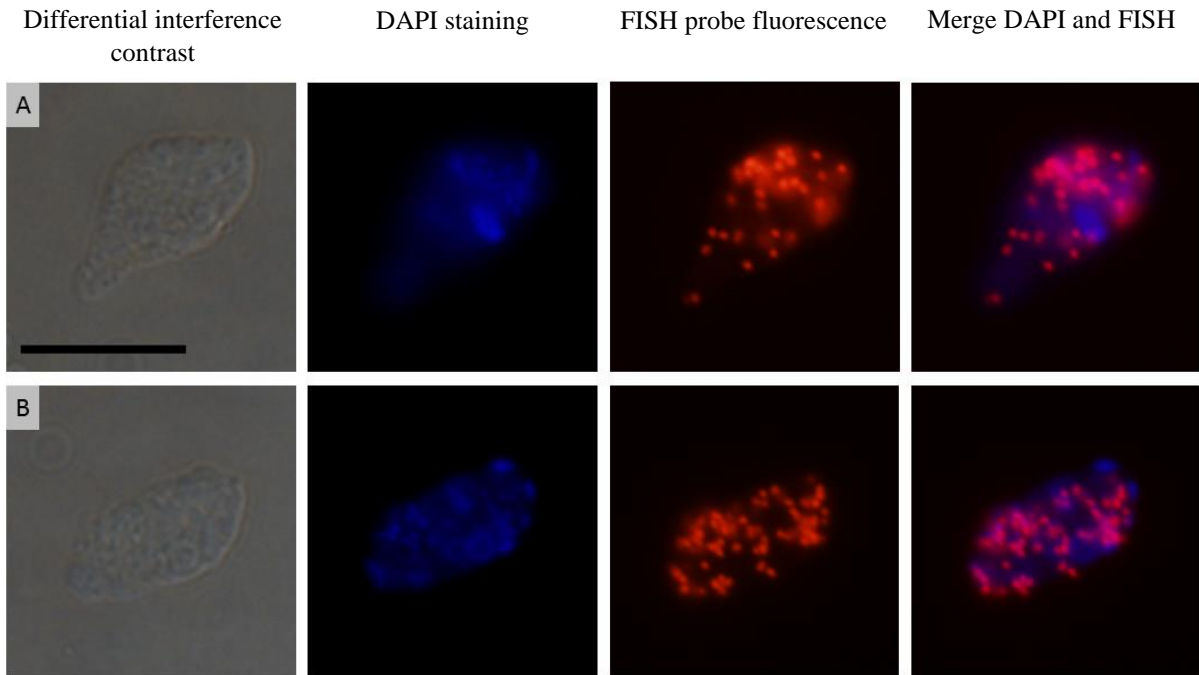


Figure 14: Differential interference contrast and fluorescence micrographs of KQ12 cells (A, B). Shown from left to right are a differential interference contrast image, DAPI staining, FISH probe fluorescence, and overlaid DAPI and FISH images. Scale bar is 10 μ m.

4.4 Molecular phylogeny and taxonomy of endosymbionts

16S rRNA PCR amplification revealed that cl. 10.3 and KQ12 possess endosymbionts. Phylogenetic analysis of the 16S rRNA genes of the endosymbionts isolated from cl. 10.3 and KQ12 confirmed their alphaproteobacterial origin (Figure 15). Both sequences are part of the *Holosporaceae* clade. It is possible to see that endosymbionts of cl. 10.3 and KQ12 are more related than their hosts KQ12 and cl. 10 are to each other (Figure 2).

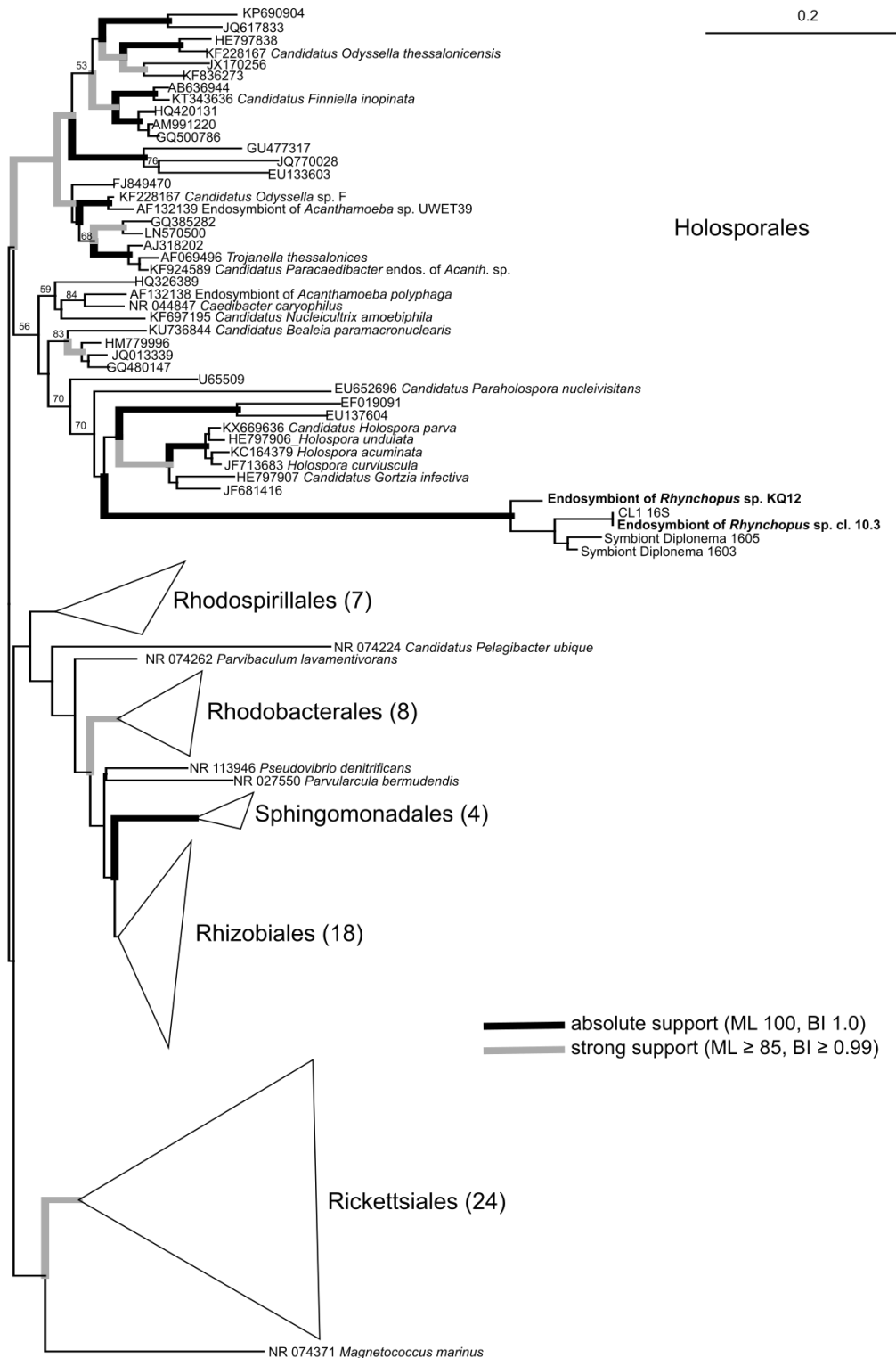


Figure 15: Maximum-likelihood (ML) phylogeny of new diplonemid-associated bacterial symbionts (bold font) based on a 16S rRNA data set containing a representative sampling of major alphaproteobacterial lineages with a focus on *Holosporaceae* inferred in RAxML 8.2.11 under the gamma-corrected GTR model. Bold lines represent absolute support (100 BS/1.0 PP).

4.5 Experiments with extracellular bacteria

Through phylogenetic analyses it was discovered that extracellular bacteria surrounding YPF1806 is species *Joostella atrarenae*. The bacteria are gram-negative, aerobic and live in seawater (Kim *et al.* 2010). Bacteria from the surrounding culture medium of YPF1806 were cultivated with YPF1808 (sample without any surrounding bacteria). However, residual staining was observed in mitochondria of YPF1808 and thus, it was inconclusive as to whether *Lacrimia* were ingesting bacteria (Figure 16).

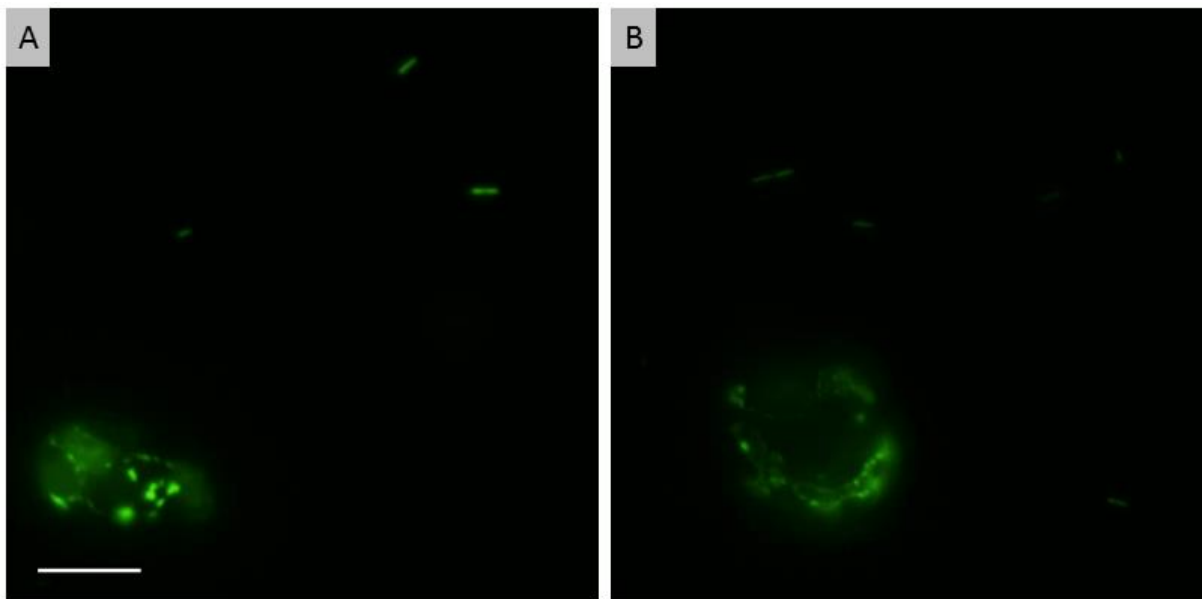


Figure 16: SYTO24 staining of extracellular bacteria and mitochondria (A, B). Scale bar is 10 μ m.

4.6 Fluorescence staining of mitochondria

Fluorescent staining of mitochondria was done either with SYTO24 stain or via an immunofluorescence assay targeting against ATPase. SYTO24 stain was successful for KQ12 (Figure 17) and YPF1808 (Figure 18). For cl. 9 (Figure 19A, B) and cl. 10 (Figure 19C, D), immunofluorescence against ATPase proved successful. Mitochondrial DNA of KQ12 appears to form isolated aggregates (Figure 17A, B) while mitochondrial DNA of YPF1808 appears to form isolated aggregates (Figure 18A) and network (Figure 18B). Mitochondrial DNA of Cl. 9 and cl. 10 also seem to form isolated aggregates (Figure 19).

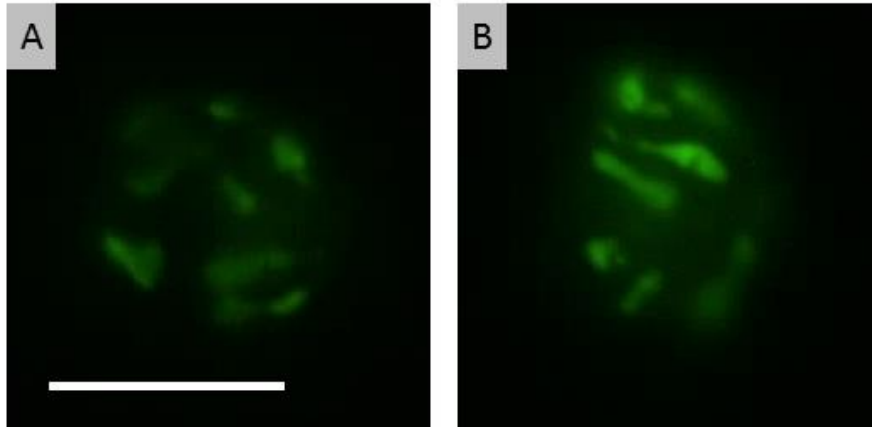


Figure 17: SYTO24 staining of mitochondria in living KQ12 cells (A, B). Scale bar is 10 μ m.

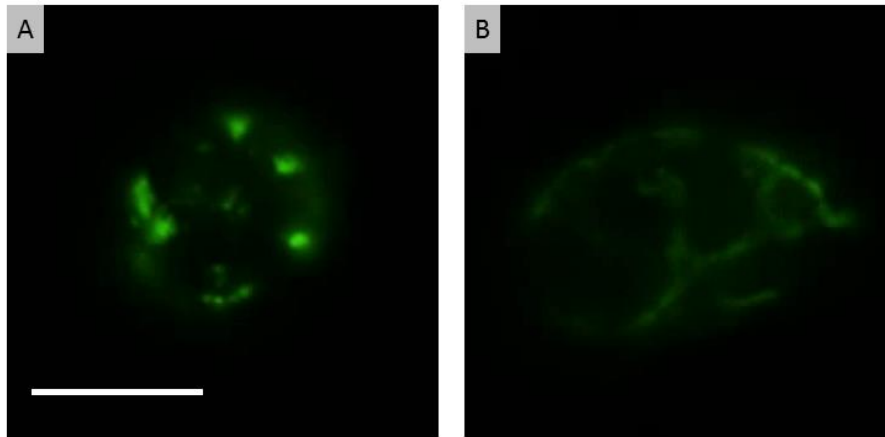


Figure 18: SYTO24 staining of mitochondria in living YPF1808 cells (A, B). Scale bar is 10 μ m.

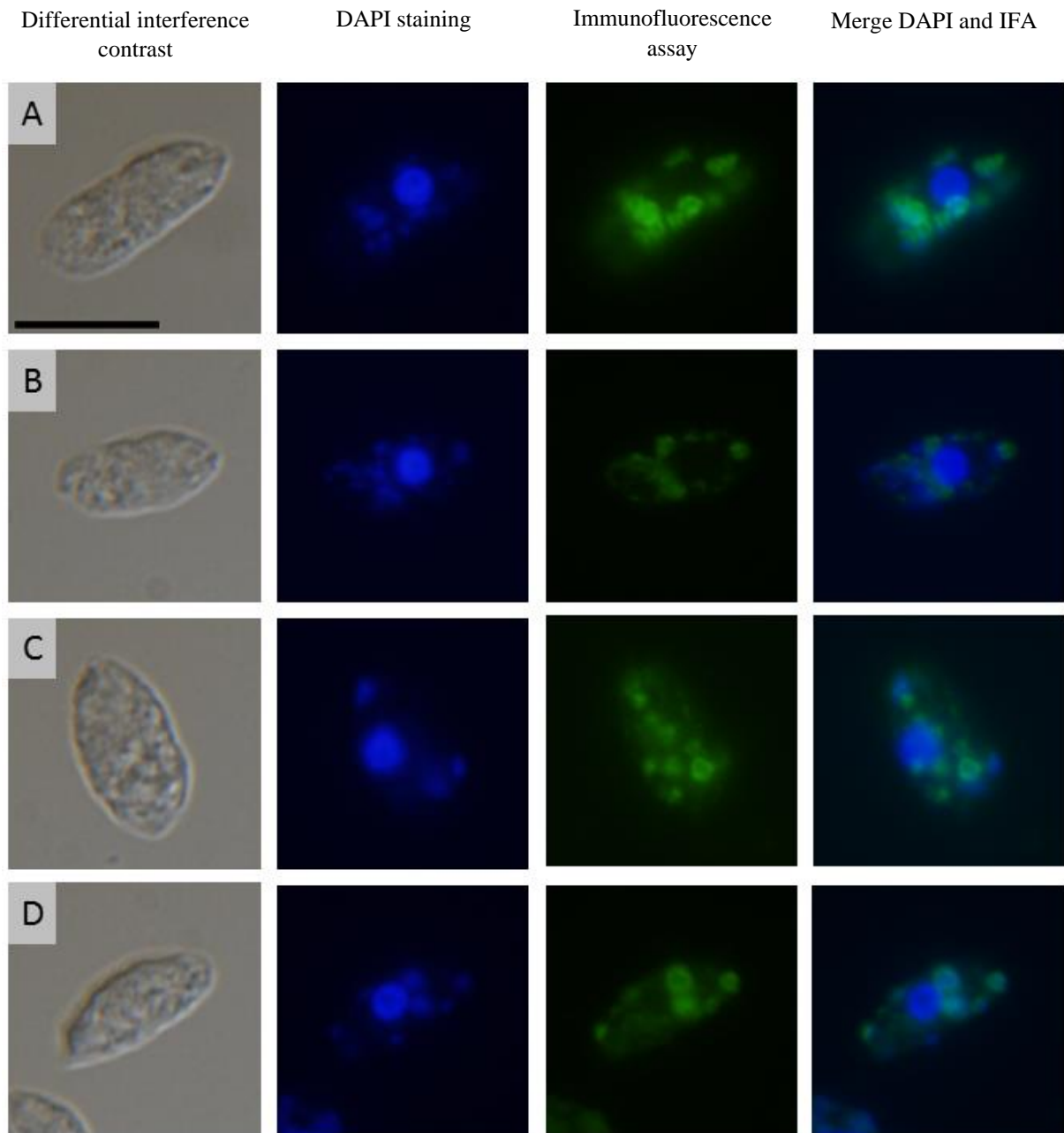


Figure 19: Differential interference contrast and fluorescence micrographs of cl. 9 (A, B) and cl. 10 (C, D). Shown from left to right are a differential interference contrast image, DAPI staining, immunofluorescence assay, and overlaid DAPI image and image from immunofluorescence assay. Scale bar is 10 μ m.

4.7 Fine structure

Scanning electron microscopy (SEM) showed that the cell surfaces of cl. 1.7 (Figure 20), cl. 10.3 (Figure 21), cl. 9 (Figure 22) and 1808 (Figure 23) are generally smooth, displaying separated feeding apparatus and a flagellar pocket which are connected with the apical papilla

at the anterior end. YPF1808 also exhibits two flagella. It was not possible to observe flagella at cl. 1.7, cl. 10.3 and cl. 9.

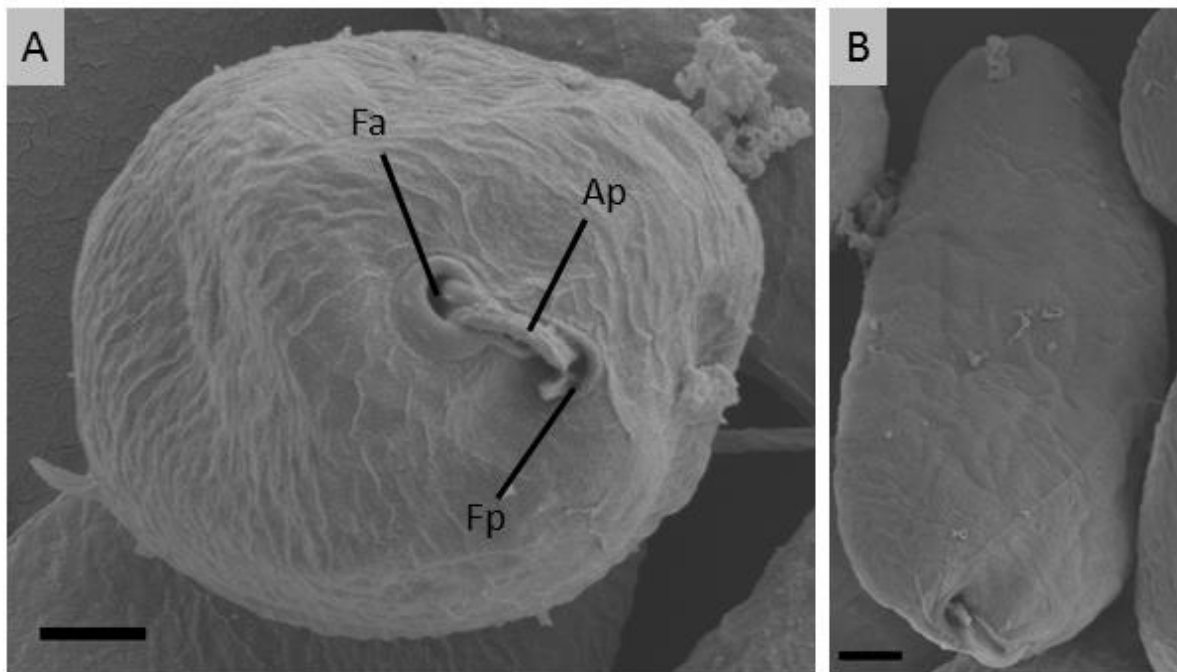


Figure 20: Scanning electron microscopy of cl. 1.7. (A) Anterior part with feeding apparatus; note the feeding apparatus (Fa), apical papilla (Ap) and flagellar pocket (Fp). (B) General appearance of the cell. Scale bar is 1µm.

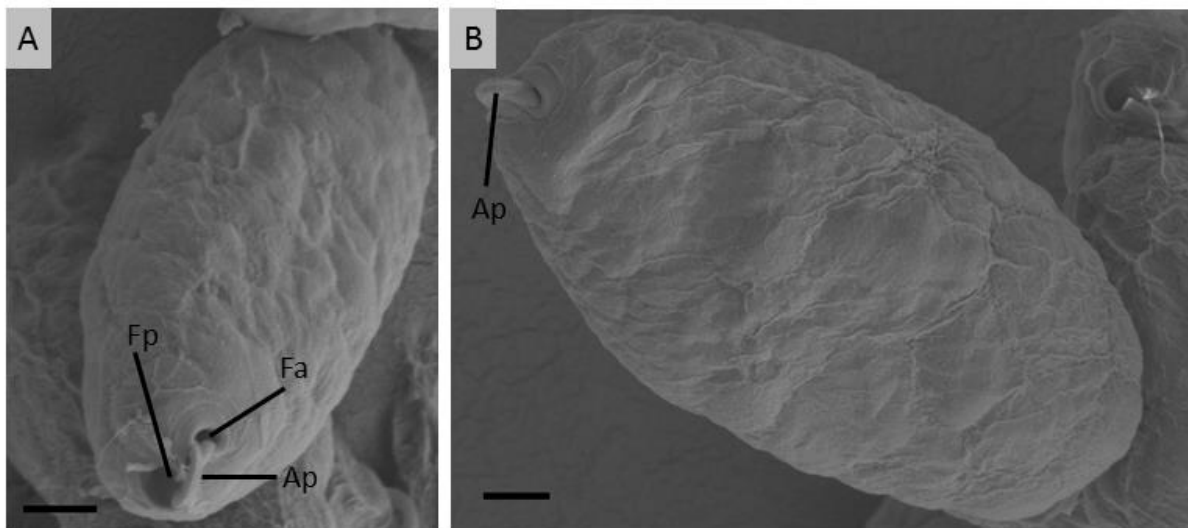


Figure 21: Scanning electron microscopy of cl. 10.3. (A, B) General appearance of the cell; note the feeding apparatus (Fa), apical papilla (Ap) and flagellar pocket (Fp). Scale bar is 1µm.

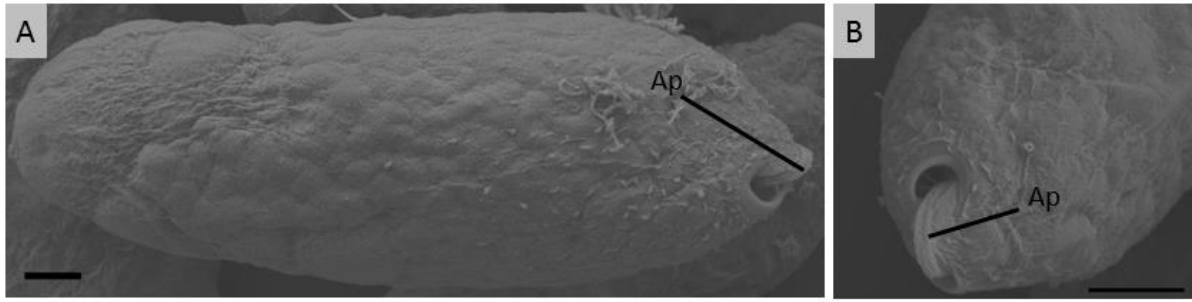


Figure 22: Scanning electron microscopy of cl. 9. (A) General appearance of the cell. (B) Anterior part with feeding apparatus; note the apical papilla (Ap). Scale bar is 1 μ m.

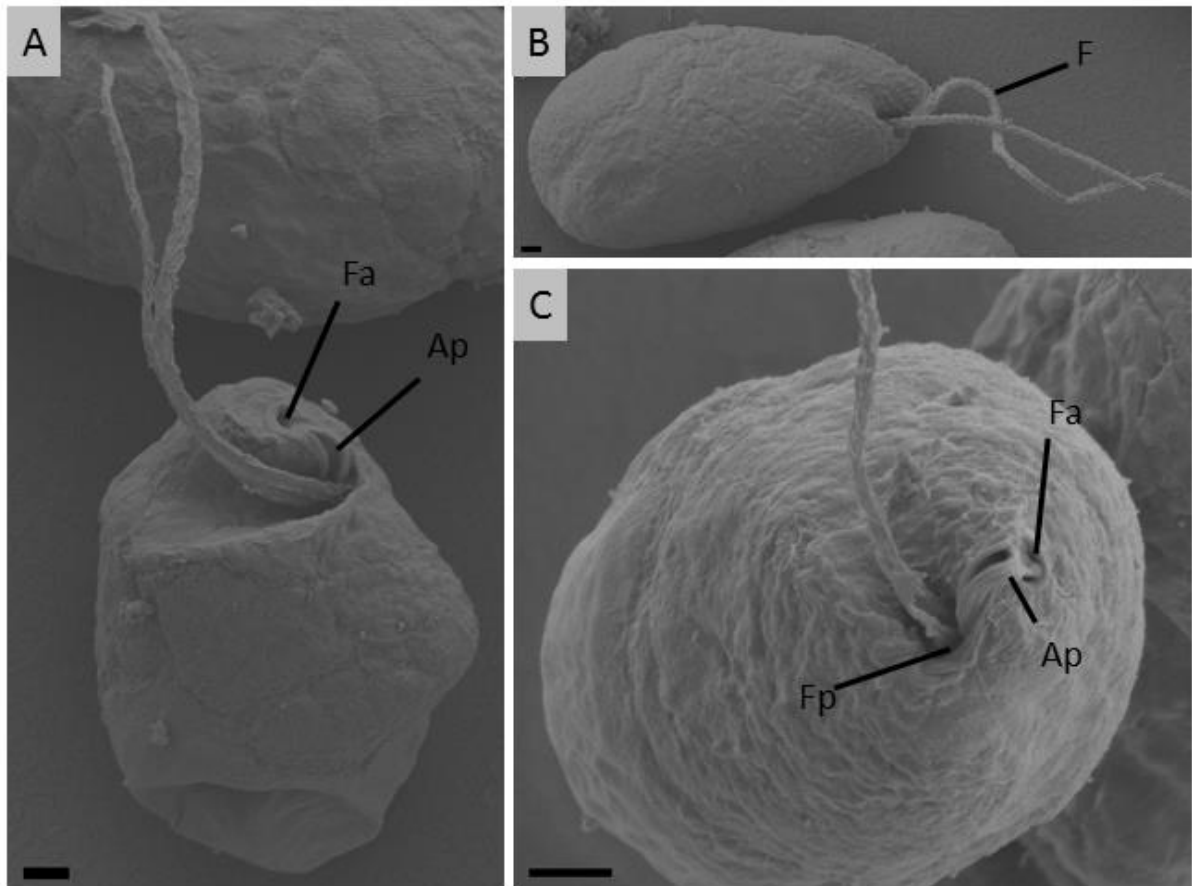


Figure 23: Scanning electron microscopy of YPF1808. (A, B) General appearance of the cell. (C) Anterior part with feeding apparatus. Note the feeding apparatus (Fa), apical papilla (Ap), flagellar pocket (Fp) and flagella (F). Scale bar is 1 μ m.

Transmission electron microscopy (TEM) revealed many organelles and inner structures in cl. 10 (Figure 24). Beneath the cell membrane lies a single-layer corset of evenly spaced microtubules joined by lateral bridges. Mitochondria vary in size and display characteristically large lamellar cristae. Longitudinally sectioned cells showed that the flagellar pocket is deep and displays two typically buried flagella. The cytopharynx extends halfway through the cell.

The Cytopharynx is tubular and curved at the cytoplasmic end. The nucleus is usually large and spherical restricted from the cytoplasm by a nuclear membrane. Golgi apparatuses are normally located near nucleus displaying cisternae and transport vesicles around it. Many endosymbiotic bacteria are randomly distributed through the cytoplasm. Cells of cl. 10 also have a large number of vacuoles (Figure 24).

Transmission electron microscopy of YPF1806 (Figure 25) revealed similar organelles and structures as those within cl. 10. Intriguingly however, an unknown structure was discovered in this species, potentially resembling a novel organelle. The novel organelle is membrane structured and appears to be in most of the cells of this *Lacrimia* species. Overall, the internal system appears to be large membrane network of connected sac-like structures. This organelle appears to have a mostly globular shape with inner structures which form concentric circles. Nonetheless, some of these inner structures form shapes of oval rings with a hollow centre. More than one of these organelles can be found per cell. Spherical spaces were observed within this organelle in YPF1808, however TEM section cells of YPF1808 were observed lysing, and thus this likely represents an artefact of preparation. The function of the novel organelle is yet unknown. Vacuoles of YPF1806 are typically full of bacteria from surrounding environment while YPF1808 do not have any bacteria in vacuoles. No endosymbiont bacteria are observed in YPF1808 or YPF1806. The nucleus is usually large and spherical, restricted from the cytoplasm by a nuclear membrane. A densely granular nucleolus is typically located in the centre of the nucleus. The nucleolus is surrounded by dense aggregations of chromatin. YPF1806 and YPF1808 are usually displaying larger vacuoles than those seen in cl. 10. Nevertheless, other organelles and structures are very similar to cl. 10. Although, YPF1808 TEM samples were observed lysing, and thus display several morphological artefacts, it was decided to display TEM pictures as it was still possible to view interesting details.

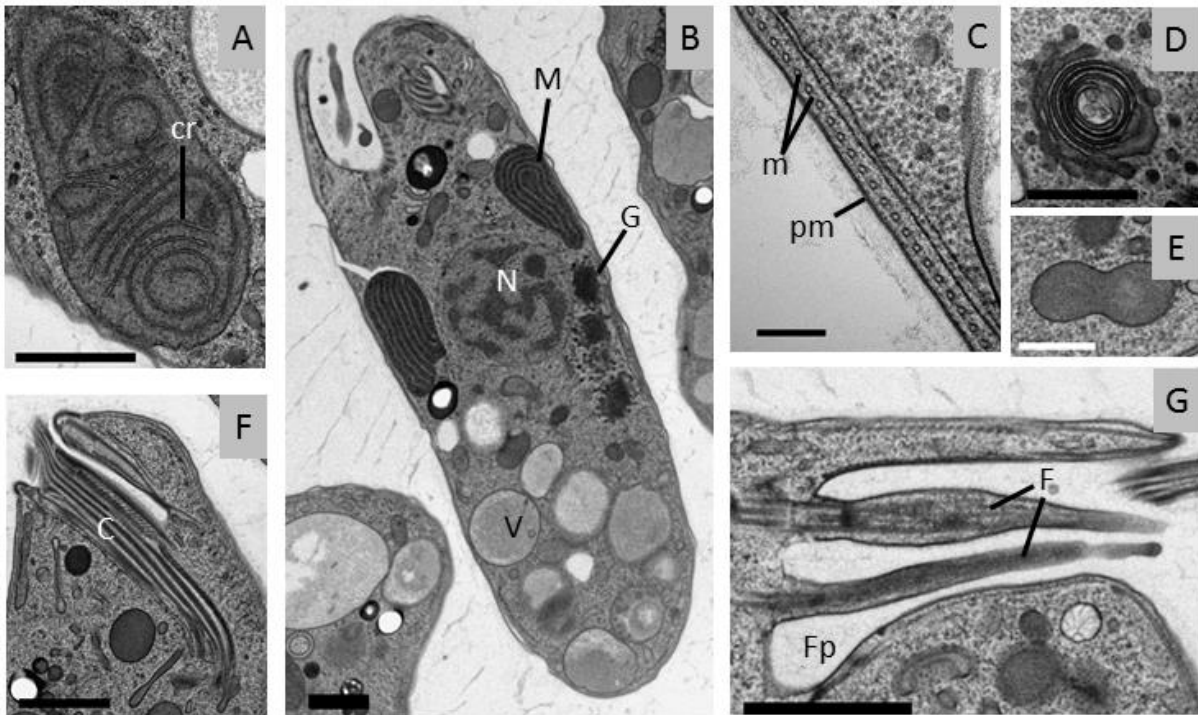


Figure 24: Transmission electron microscopy of cl. 10. (B) Longitudinally sectioned cell illustrating the main ultrastructural features; note the nucleus (N), mitochondrion (M), Golgi apparatus (G) and vacuole (V). (A) Mitochondrion displaying characteristic large lamellar cristae (cr). (C) Cross section demonstrating plasma membrane (pm) and single row of microtubular corset (m) underneath it. (D) Detail of Golgi apparatus. (E) Dividing endosymbiotic bacteria. (F) Longitudinal section through the cytopharynx. (G) Longitudinal sections through flagella (F) and the area of flagellar attachment; note the flagellar pocket (Fp). Scale bars: 1 μ m (A, B, G, F); 0.5 μ m (D, E) and 0.2 μ m (C).

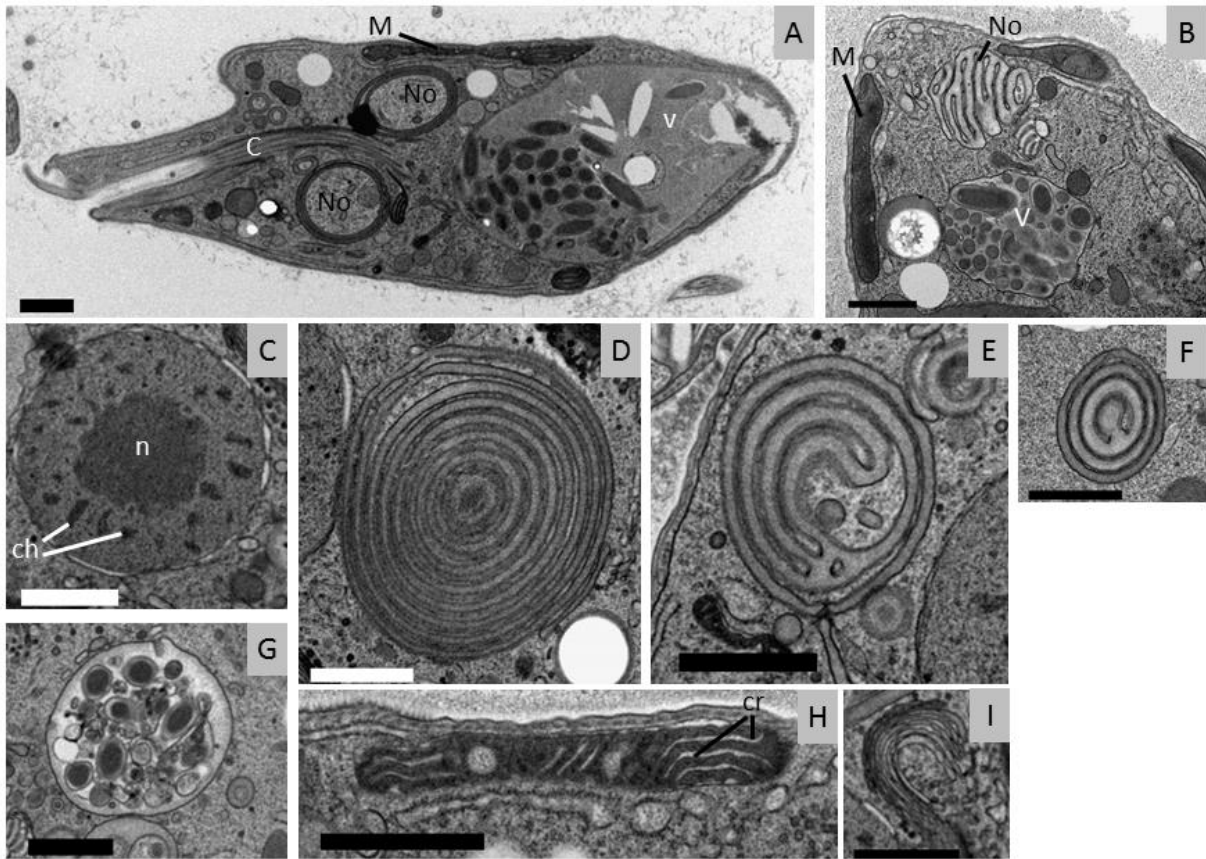


Figure 25: Transmission electron microscopy of YPF1806. (A) Longitudinally sectioned cell illustrating the main ultrastructural features; note the cytopharynx (C), mitochondrion (M) and vacuole (V) with bacteria. (B) Detailed section of YPF1806, note the mitochondrion (M), vacuole (V) with endosymbiont and Novel organelle (No). (C) Section through large nucleus. Centrally located nucleolus is surrounded by dense aggregations of chromatin (ch). (D, E, F) New organelle with membrane structures. (G) Detail of vacuole with bacteria. (H) Mitochondrion displaying characteristic large lamellar cristae (cr). (I) Detail of Golgi apparatus. Scale bars are 1 μ m.

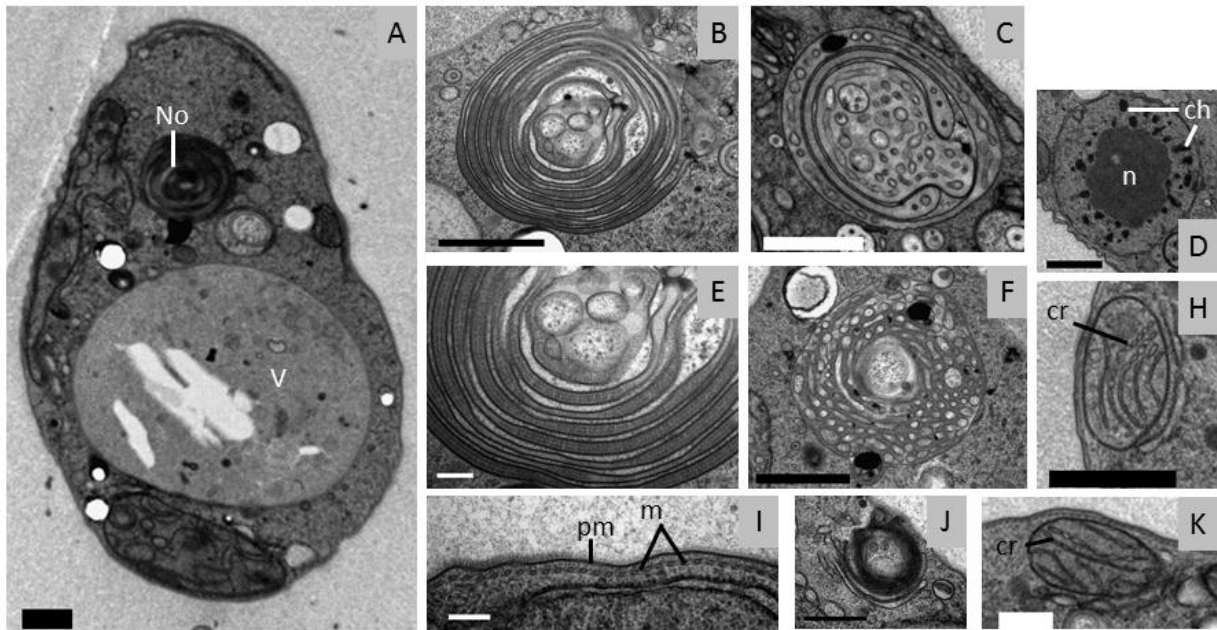


Figure 26: Transmission electron microscopy of lysed YPF1808. (A) Longitudinally sectioned cell illustrating the main ultrastructural features; note the large posterior vacuole (V) without bacteria and novel organelle (No). (B, C, E, F) Novel organelle with membrane structures. (E) Detail of novel organelle. (C, F) Pictures of novel organelles which may be in lysis. (D) Section through large nucleus. Centrally located nucleolus is surrounded by dense aggregations of chromatin (ch). (H, K) Lysing mitochondria displaying large lamellar cristae (cr); note that cristae are twisted. (I) Cross section demonstrating plasma membrane (pm) and single row of microtubular corset (m) underneath it. (J) Detail of Golgi apparatus. Scale bars: 1 μm (A, B, C, D, F, H); 0.5 μm (J, K) and 0.2 μm (E, I).

5 Discussion

Phylogenetic analysis confirmed four new diplonemid species from this study. Identical YPF1808 and YPF1806 species belong into the *Lacrimia* genus while identical cl. 10.3 and cl. 1.7 belong into the *Rhynchopus* genus. Species KQ12 and cl. 9 also belong into the *Rhynchopus* genus.

Phylogenetic analyses of bacterial endosymbionts revealed that both endosymbionts are new species and are members of family *Holosporaceae*, of which previously studied diplonemid endosymbionts also belong to (Tashyreva *et al.* 2018b). Diplonemids which were studied to the date have been found hosting primarily alphaproteobacteria. In contrast, distantly related members Kinetoplastea, particularly trypanosomatids of the genera *Strigomonas* and *Angomonas* harbour endosymbiotic betaproteobacteria. (Alves *et al.* 2013), (Tashyreva *et al.* 2018b).

Results from cell measurements suggest that bacterial endosymbionts may have an impact on the length of cl. 10.3 and cl. 1.7, as it was observed that cl. 1.7, without endosymbionts, is on average 1.3 μ m longer than cl. 10.3. However, it is acknowledged that this assessment is based on a limited dataset (n=50) and the observed differential may be within the error bounds associated with the measurements.

It appears that neither bacterial endosymbionts nor extracellular bacteria have a significant influence on the growth rates of chosen diplonemids species. A previous study (Gast *et al.* 2009) suggested that endosymbionts of protists can play a role in supplementing nutrition. If this was true in our studied diplonemids, we would expect growth curve of cl. 1.7 and 10.3 to differ. No substantial difference in growth curve of YPF1808 and YPF1806 was observed, suggesting that this species of *Lacrimia* is not affected by these bacteria, either as a hindrance or benefit, and would additionally suggest that this diplonemid species may not be using these bacteria as a food source.

Previous experiments (Tashyreva *et al.* 2018b) indicated that when *Diplonema japonicum* were placed in starvation medium, cells went first through a sessile stage and after 24 hours they transitioned into a swimming stage which lasted about 12 hours. Starvation experiments in the current study showed that cl. 10.3, cl. 1.7 and KQ12 also display similar swimming stages under appropriate conditions. However, only a few swimming cells were observed in starved cultures. It was not possible to observe the swimming stage in cl. 9. However, many earlier

examined *Rhynchopus* species displayed swimming stages (Tashyreva *et al.* 2018a) which would suggest that cl. 9 might develop a swimming stage under different conditions. There were no observed differences between cl. 10.3 and cl. 1.7, except that on the sixth day post-starvation, a few swimming cells were observed in cl. 10.3 but not in 1.7. Nevertheless, swimming cells were observed very rarely so there is a possibility that they could be swimming in flasks with cl. 1.7 as well but were too rare to be observed. This further suggests that bacterial endosymbionts additionally do not impact life stage transitions in this species. However, in other studies, it was found that after two weeks of starvation, the number of endosymbionts in diplomonids decreased (Tashyreva *et al.* 2018b), which suggests a sophisticated relationship between host and endosymbiont. Additionally, there were no observed differences between YPF1806 and YPF1808 regarding the development of fast swimming cells which implies that this species of extracellular bacteria does not influence swimming behaviour in the *Lacrimia* species.

Endosymbiotic bacteria were observed in two *Rhynchopus* species – cl 10.3 and KQ12. Their function within the hosts are still unknown. We had the opportunity to compare the same species with (cl. 10.3) and without (cl. 1.7) endosymbionts. The comparison showed a lack of noticeable differences in life cycle transitions between these otherwise identical samples which suggests that endosymbionts do not meaningfully impact this *Rhynchopus* species when in an artificial laboratory environment. It remains a possibility however that endosymbionts may be important for their diplomonid hosts when in their natural oceanic habitats.

Comparisons of YPF1808 and YPF1806 suggest that extracellular bacteria do not have any larger effects on their life cycle. From transmission electron microscopy it was possible to see YPF1806 ingesting extracellular bacteria, but we do not observe evidence that this species is feeding and gaining nutrition from them.

Fluorescence staining with different techniques was necessary due to different species having different structural features affecting the success of various procedures. Accordingly, YPF1808 and KQ12 stained successfully with SYTO24 while cl. 9 and cl. 10 had to be stained via immunofluorescence assay.

Scanning electron microscopy did not reveal any new structural features which were not described in previous studies (Tashyreva *et al.* 2018a, Tashyreva *et al.* 2018b). Interestingly however, transmission electron microscopy revealed a putative novel organelle in the newly defined *Lacrimia* species, although its function remains unknown.

For future studies, it would may be interesting to try new distinct brands of sea salts and various amounts of nutrition in medium for various species as cultivation proved challenging for several species. Varied types of sea salts could be also used to potentially introduce a greater proportion of swimming cells and/or provoke a swimming stage in cl. 9. It would additionally be interesting to try embedding cells in agarose gel with small amount of nutrition media on the top of agarose as a means of stimulating swimming cells, as was successfully demonstrated in prior studies (Tashyreva *et al.* 2018a). Finally, further studies and experiments will have to be completed to identify the novel organelle which was found in the *Lacrimia* species YPF1808 and YPF1806.

6 References

- David V & Archibald JM (2016). Evolution: Plumbing the Depths of Diplonemid Diversity. *Current Biology* 26:R1290–R1292. <https://doi.org/10.1016/j.cub.2016.10.050>
- Lukeš J, Flegontova O & Horák A (2015). Diplonemids. *Current Biology* 25:R702-R704. <https://doi.org/10.1016/j.cub.2015.04.052>
- Flegontova O, Flegontov P, Malviya S, Audic S, Wincker P, de Vargas C, Bowler C, Lukeš J & Horák A (2016). Extreme Diversity of Diplonemid Eukaryotes in the Ocean. *Current Biology* 26:3060-3065. <https://doi.org/10.1016/j.cub.2016.09.031>
- Tashyreva D, Prokopchuk G, Yabuki A, Kaur B, Faktorová D, Votýpka J, Kusaka C, Fujikura K, Shiratori T, Ken-Ichiro I, Horák A & Lukeš J (2018a). Phylogeny and Morphology of New Diplonemids from Japan. *Protist* 169:158-179. <https://doi.org/10.1016/j.protis.2018.02.001>
- Tashyreva D, Prokopchuk G, Votýpka J, Yabuki A, Horák A & Lukeš J (2018b). Life Cycle, Ultrastructure, and Phylogeny of New Diplonemids and Their Endosymbiotic Bacteria. *mBio* 9:02447-17. <https://doi.org/10.1128/mBio.02447-17>
- Burger G & Valach M (2018). Perfection of eccentricity: Mitochondrial genomes of diplonemids. *IUBMB Life* 70:1197-1206. <https://doi.org/10.1002/iub.1927>
- Faktorová D, Dobáková E, Peña-Díaz P & Lukeš J (2016). From simple to supercomplex: mitochondrial genomes of euglenozoan protists. [version 2; peer review: 2 approved]. *F1000Research* 5:392. <https://doi.org/10.12688/f1000research.8040.2>
- Hampl V, Hug L, Leigh JW, Dacks JB, Lang BF, Simpson AGB & Roger AJ (2009). Phylogenomic analyses support the monophyly of Excavata and resolve relationships among eukaryotic “supergroups”. *Proceedings of the National Academy of Sciences* 106:3859-3864. <https://doi.org/10.1073/pnas.0807880106>
- Simpson AGB (1997). The identity and composition of the Euglenozoa. *Archiv für Protistenkunde* 148:318-328. [https://doi.org/10.1016/S0003-9365\(97\)80012-7](https://doi.org/10.1016/S0003-9365(97)80012-7)
- Gibson W (2016). Kinetoplastea. In: Archibald J. et al. (eds) *Handbook of the Protists*. Cham: Springer International Publishing AG. pp. 1-2. https://doi.org/10.1007/978-3-319-32669-6_7-1

Kottuparambil S, Thankamony RL & Agusti S (2019). Euglena as a potential natural source of value-added metabolites. A review. *Algal Research* 37:154-159. <http://dx.doi.org/10.1016/j.algal.2018.11.024>

Yabuki A & Tame A (2015). Phylogeny and Reclassification of *Hemistasia phaeocysticola* (Scherffel) Elbrächter & Schnepf, 1996. *The Journal of Eukaryotic Microbiology* 62:426-429. <https://doi.org/10.1111/jeu.12191>

George EE, Husnik F, Tashyreva D, Prokopchuk G, Horák A, Kwong WK, Lukeš J & Keeling PJ (2020). Highly Reduced Genomes of Protist Endosymbionts Show Evolutionary Convergence. *Current Biology* 30:925-933. <https://doi.org/10.1016/j.cub.2019.12.070>

Kearse M, Moir R, Wilson A, Stones-Havas S, Cheung M, Sturrock S, Buxton S, Cooper A, Markowitz S, Duran C, Thierer T, Ashton B, Meintjes P & Drummond A (2012). Geneious Basic: An integrated and extendable desktop software platform for the organization and analysis of sequence data. *Bioinformatics (Oxford, England)* 28:1647–1649. <https://doi.org/10.1093/bioinformatics/bts199>

Katoh K & Standley DM (2013). MAFFT Multiple SequenceAlignment Software version 7: improvements in performanceand usability. *Molecular Biology and Evolution* 30:772–780. <https://doi.org/10.1093/molbev/mst010>

Talavera G & Castresana J (2007). Improvement of phylogenies after removing divergent and ambiguously aligned blocks from protein sequence alignments. *Systematic Biology* 56, 564-577. <https://doi.org/10.1080/10635150701472164>

Stamatakis A (2014). RAxML version 8: a tool for phylogenetic analysis and post-analysis of large phylogenies. *Bioinformatics* 30:1312-1313. <https://doi.org/10.1093/bioinformatics/btu033>

Prokopchuk G, Tashyreva D, Yabuki A, Horák A, Masařová P & Lukeš J (2019). Morphological, Ultrastructural, Motility and Evolutionary Characterization of Two New Hemistasiidae Species. *Protist* 170:259-282. <https://doi.org/10.1016/j.protis.2019.04.001>

Small EB & Marszalek DS (1969). Scanning electron microscopy of fixed, frozen, and dried protozoa. *Science* 163:1064–1065. <https://doi.org/10.1126/science.163.3871.1064>

Kim BC, Lee KH, Kim MN, Jung MY, Chang Y, Lee J & Shin KS (2011). *Joostella atrarenae* sp. nov., a novel member of the *Flavobacteriaceae* originating from the black sea sand of Jeju Island. *Current Microbiology* 62:606-611. <https://doi.org/10.1007/s00284-010-9750-y>

Yurchenko V, Votýpka J, Tesařová M, Klepetková H, Kraeva N, Jirků M & Lukeš J (2014). Ultrastructure and molecular phylogeny of four new species of monoxenous trypanosomatids from flies (Diptera: *Brachycera*) with redefinition of the genus *Wallaceina*. *Folia Parasitologica* 61:97–112. DOI: [10.14411/fp.2014.023](https://doi.org/10.14411/fp.2014.023)

Alves JM, Klein CC, da Silva FM, Costa-Martins AG, Serrano MG, Buck GA, Vasconcelos ATR, Sagot MF, Teixeira MM, Motta MCM & Camargo EP (2013). Endosymbiosis in trypanosomatids: the genomic cooperation between bacterium and host in the synthesis of essential amino acids is heavily influenced by multiple horizontal gene transfers. *BMC Evolutionary Biology* 13:190. <https://doi.org/10.1186/1471-2148-13-190>

Gast RJ, Sanders RW & Caron DA (2009). Ecological strategies of protists and their symbiotic relationships with prokaryotic microbes. *Trends in Microbiology* 17:563-569. <https://doi.org/10.1016/j.tim.2009.09.001>